

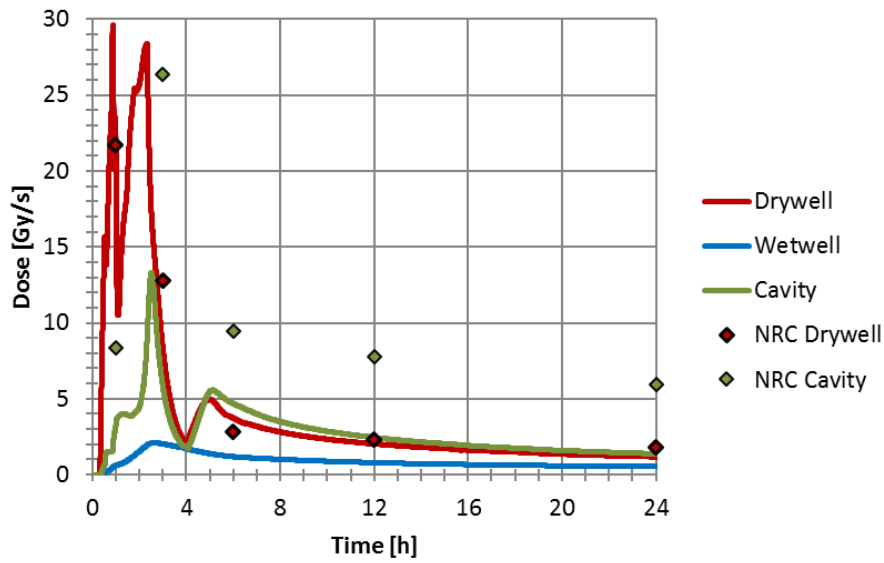
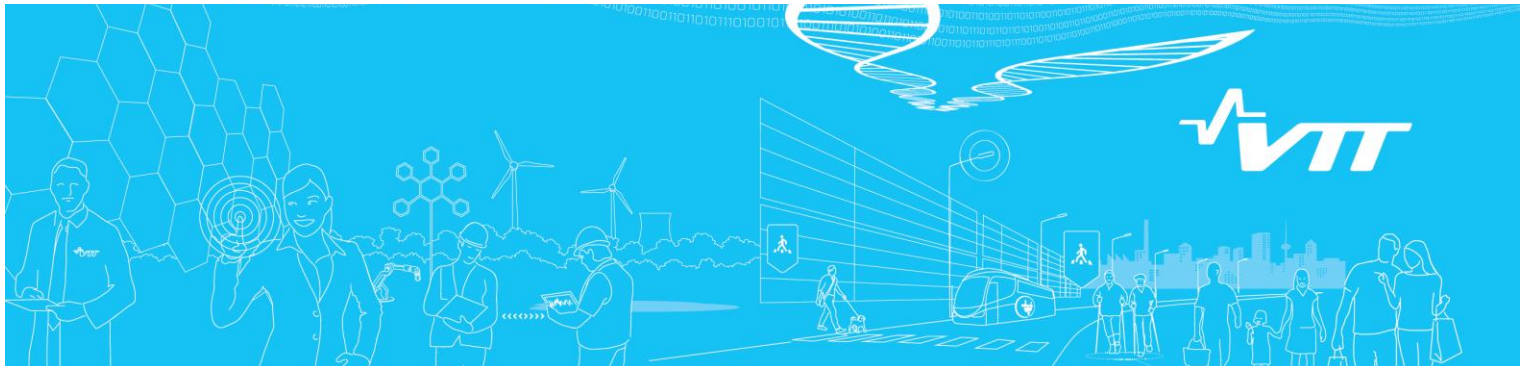
Title	Comparing in-containment dose rates calculated with ASTEC and NRC method
Author(s)	Nieminen, Anna; Rossi, Jukka
Citation	RESEARCH REPORT : VTT-R-00760-17 VTT, 2017, pages 31 + 8 app.
Rights	This report may be downloaded for personal use only.

VTT
<http://www.vtt.fi>
P.O. box 1000
FI-02044 VTT
Finland

By using VTT Digital Open Access Repository you are bound by the following Terms & Conditions.

I have read and I understand the following statement:




This document is protected by copyright and other intellectual property rights, and duplication or sale of all or part of any of this document is not permitted, except duplication for research use or educational purposes in electronic or print form. You must obtain permission for any other use. Electronic or print copies may not be offered for sale.



Comparing in-containment dose rates calculated with ASTEC and NRC method

Authors: Anna Nieminen, Jukka Rossi

Confidentiality: Public

Report's title	
Comparing in-containment dose rates calculated with ASTEC and NRC method	
Customer, contact person, address	Order reference
SAFIR2018 Research Programme	SAFIR 6/2016
Project name	Project number/Short name
Comprehensive Analysis of Severe Accidents	108735 / CASA
Author(s)	Pages
Anna Nieminen, Jukka Rossi	31 + App. 8
Keywords	Report identification code
severe accident, dose rate, ASTEC	VTT-R-00760-17
Summary	
<p>Estimating the dose rates inside the containment during a hypothetical severe accident is important since the radiation dose might affect the operation of instrumentation and automation systems and the leak-tightness of containment penetration seal materials. Dose rate affects also the formation of nitric acid in the containment that reduces the pool pH decreasing iodine retention in pools.</p> <p>The objective of this work was to compare the dose rates in containment produced by integral code ASTEC and by NRC method. The selected test case was a large LOCA in a Nordic BWR. The source term to the containment was defined based on NUREG-1465 report. Fission product distribution for NRC method dose calculations was obtained from ASTEC.</p> <p>The gas phase dose rates produced by NRC method were expected to be higher than the ASTEC dose rates because, in the NRC method, the deposited fission products were included in the gas phase inventory, and because ASTEC assumes that 50 % of the radiation from the deposited fission products is absorbed by the wall.</p> <p>This assumption was more or less confirmed, but the difference was higher than expected for all but drywell beta dose rate. It is assumed that ASTEC does not take into account the decreasing gas phase volume due to cavity flooding when defining the dose rate. However, in all cases the total dose rate estimates were within a factor of two that can be considered rather acceptable difference taking into account different approach in the methods.</p> <p>ASTEC input was also changed by increasing the wet painted wall area in the containment. It was expected that this would increase the mass of organic iodide, but it increased more notably the mass of I₂ and iodine oxides. The change in iodine behaviour resulted slightly higher dose peaks in the containment gas phase but notably smaller dose rates on walls.</p>	
Confidentiality	Public
Espoo 10.2.2017	
Written by	Reviewed by
	
Anna Nieminen, Research Scientist	Tuomo Sevón, Senior Scientist
Accepted by	
Anitta Hämäläinen, Research Team Leader	
VTT's contact address	
VTT, P.O.Box 1000, 02044 VTT, Finland	
Distribution (customer and VTT)	
SAFIR2018 Reference Group 2, Jari Hämäläinen (VTT), Vesa Suolanen (VTT), Tuomo Sevón (VTT), Anitta Hämäläinen (VTT)	
<p><i>The use of the name of VTT Technical Research Centre of Finland Ltd in advertising or publishing of a part of this report is only permissible with written authorisation from VTT Technical Research Centre of Finland Ltd.</i></p>	

Contents

Contents.....	2
1 Introduction.....	3
2 Fission product behaviour.....	3
2.1 Release and transportation in primary circuit.....	3
2.2 Aerosols.....	4
2.3 Iodine chemistry in containment.....	5
2.3.1 Liquid phase chemistry.....	6
2.3.2 Gas phase chemistry and retention of iodine.....	6
3 ASTEC V2.1.....	6
3.1 SOPHAEROS module.....	7
3.2 DOSE and ISODOP modules.....	8
4 NRC method for defining the dose rate.....	9
4.1 Dose rate in the gas phase.....	10
4.2 Dose rate in water.....	10
5 ASTEC input deck.....	11
5.1 Containment and boundary conditions.....	11
5.2 Fission product part.....	14
6 Results.....	14
6.1 Thermal hydraulic behaviour.....	14
6.2 The produced dose rates.....	18
6.3 Fission product behaviour.....	22
6.3.1 Comparison to previous results.....	27
7 Discussion and conclusions.....	29
References.....	30
Appendix A.....	32

1 Introduction

The focus on analysing fission product behaviour in containment during a severe accident has been on aerosol physics and iodine chemistry (Simondi-Teisseire et al., 2013; Funke et al., 2012; Glowa and Moore, 2011; Colombani et al., 2011). The main objective has been to define the potential source term to the environment as accurately as possible. Dose rate has been part of these analyses only when estimating its effect on iodine chemistry for example radiolytic oxidation of molecular iodine (Bosland et al., 2011). The overall dose rates have been mostly defined when considering environmental consequences.

Estimating the dose rates inside the containment during a hypothetical severe accident is important since the radiation dose might affect the operation of instrumentation and automation systems and leak-tightness of containment penetration seal materials. To be able to assess the operation of these systems and structures in all circumstances, reliable evaluations on fission product behaviour in the containment are needed. Dose rate affects also the formation of nitric acid (HNO_3) in the containment that reduces the pool pH decreasing iodine retention in pools.

The objective of this work was to compare the dose rates in containment produced by integral code ASTEC (Accident Source Term Evaluation Code) (Chatelard et al., 2015) and by NRC method (NRC, 1972). The selected test case was a large LOCA (Loss of Coolant Accident) in a Nordic BWR (Boiling Water Reactor) plant. The source term to the containment was defined based on NUREG-1465 report (Soffer et al., 1995) published for regulatory application.

2 Fission product behaviour

Dose rates depend firstly on fission product release. What is the amount of each released element and when they are released? Secondly, fission product behaviour in the containment affects dose rates largely. How fission products are transported between different rooms, which elements are dissolved in water and what is the amount of deposited aerosols? Therefore, it is important to be familiar with the principles of fission product behaviour to understand what the origin of dose rate is.

In 1995 the U.S Nuclear Regulatory Commission (NRC) published NUREG-1465 "Accident Source Terms for Light-Water Nuclear Power Plants" that presents representative in-containment fission product source terms for BWRs and PWRs (Pressurized Water Reactors). Since then, several experimental programmes have analysed fission product release and behavior focusing especially on iodine chemistry. One of the most important ones is Phébus FP (Clément & Zeyen, 2013).

2.1 Release and transportation in primary circuit

It is commonly assumed that 5 % of volatile fission products are located to the gas gap between fuel pellet and cladding. This inventory is immediately released when cladding fails. If accident proceeds, the fuel heats up and more volatile fission products start to accumulate to the fuel pellet grain boundaries from where they are first migrated to the pellet surface and then released. Eventually fuel degradation begins, resulting loss of fuel geometry. During this early in-vessel phase all noble gases are released as well as significant amounts of volatile nuclides.

BWR release into the containment according to NUREG-1465 is presented in Table 1. There exists a qualitative agreement between NUREG-1465 and Phébus FP data concerning gap and early in-vessel releases (Herranz & Clément, 2010). Fractions of noble gases and volatile fission products (I, Cs and Te) released into containment are consistent. However, Cs release is generally lower due to its retention in the coolant system, and Te release measurements

varied highly due to different conditions in the Phébus FP experiments and can then be higher than in NUREG-1465.

Table 1. BWR release fractions into the containment according to NUREG-1465.

Release Group	Elements	Gap release	Early In-Vessel	Ex-Vessel	Late In-Vessel
1) Noble gases	Xe, Kr	0.05	0.95	0	0
2) Halogens	I, Br	0.05	0.25	0.3	0.01
3) Alkali metals	Cs, Rb	0.05	0.2	0.35	0.01
4) Tellurium group	Te, Sb, Se	0	0.05	0.25	0.005
5) Barium, Strontium	Ba, Sr	0	0.02	0.1	0
6) Noble metals	Ru, Rh, Pd, Mo, Tc, Co	0	0.0025	0.0025	0
7) Lanthanides	La, Zr, Nd, Eu, Nb, Pm, Pr, Sm, Y, Cm, Am	0	0.0005	0.005	0
8) Cerium group	Ce, Pu, Np	0	0.0002	0.005	0
Release duration		0.5 h	1.5 h	3.0 h	10 h

Phébus-FP experiments confirmed also that iodine is transported through primary circuit both in gaseous and particulate forms. NUREG-1465 (Soffer et al., 1995) states that at least 95 % of the iodine entering to the containment is CsI and there is no more than 5 % in the gaseous forms (atomic iodine (I) and hydrogen iodide (HI)). In Phébus tests with silver-indium-cadmium control rods cadmium iodide (CdI_2) was more common form of particulate iodide than CsI (Girault & Payot, 2013).

According to NUREG-1465, after early in-vessel phase occurs ex-vessel phase and simultaneously occurs also late in-vessel phase. Ex-vessel phase starts when the reactor pressure vessel fails and core melt is released to the reactor pit. During the late in-vessel phase some of the volatile nuclides that deposited in the reactor coolant system during the core degradation and melting may re-volatilize and be released to the containment.

Caesium (Cs) has typically been assumed to be released as caesium hydroxide (CsOH) in accident analyses. NUREG-1465 does not directly instruct dealing with the chemical form of Cs. In Phébus FP experiments it was found out that Cs is actually released as caesium molybdate (Cs_2MoO_4) vapour rather than CsOH (Girault & Payot, 2013). CsOH that did reach the containment in the experiments originated from the re-vaporization of the deposited caesium in high temperature steam.

2.2 Aerosols

In addition to noble gases, only iodine and ruthenium are able to enter the containment in gaseous form in small extent. When the released volatile fission products cool down in the primary circuit, they condense and take the form of aerosol particles. Particulate materials are transported through the reactor coolant system to the containment as agglomerates of mixed substances rather than pure substances.

The presence of high humidity in the containment induces an intense condensational growth of the aerosol particles. Steam condenses on aerosol surface, and a fraction of the particle

material can become dissolved. The increase of particle size enhances the gravitational settling rate and therefore aerosol depletion through deposition on surfaces. Gravitational settling was proven to be the main depletion mechanism for aerosols in Phébus-FP experiments (Simondi-Teisseire et al., 2013).

Another mechanism contributing to enhanced deposition in the containment is diffusiophoresis, which is usually combined with thermophoresis. Diffusiophoresis is driven by a steam mass flux toward the condensing wall surfaces, whereas thermophoresis is driven by a steep temperature gradient between the containment atmosphere and the containment walls.

2.3 Iodine chemistry in containment

It can be concluded that half of the effective dose in air is due to noble gases. Different aerosols, among which iodine aerosols, and gaseous iodine are responsible of the other half (Chevalier-Jabet et al., 2014). Iodine behaviour is then very important what comes to dose rates. Despite recent research efforts, significant uncertainties are still related to iodine chemistry whereas the behaviour of aerosols and noble gases is rather straightforward. Aerosol physics is well known and noble gases are inert.

Most of the iodine enters the containment as metal-iodides. These compounds are incorporated into agglomerated aerosol particles containing other fission product and structural material. The airborne concentration of these iodine-bearing particles is governed by aerosol physics. The principles of iodine chemistry in the containment is illustrated in Figure 1. (Clément et al., 2007)

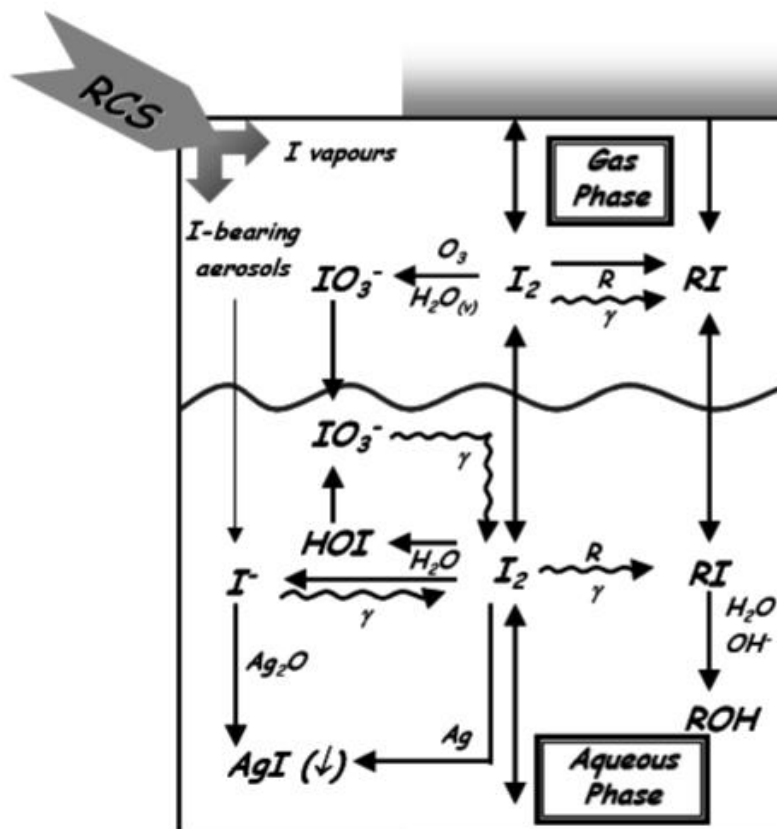


Figure 1. Illustration of iodine behaviour in the containment. (Clément et al., 2007)

2.3.1 Liquid phase chemistry

Most of the metal iodides are soluble and will be dissolved to sump water to form iodide ions that will form volatile I_2 due to radiative and thermal effects. The formation of I_2 depends extensively on pH level of the sump. If pH is controlled to be alkaline ($pH > 7$), the formation of I_2 is considered to be very low (Clément et al., 2007) because alkaline water promotes iodine hydrolysis. NUREG-1465 actually states that in this case less than 1 % of the dissolved iodine will be converted to elemental iodine.

Other source for volatile iodine in the sump is the formation of organic iodine compounds of which part are also non-volatile. Organic radicals in the sump water originate for example from paints. (Clément et al., 2007) However, in Phébus experiments the immersed paints did not play a significant role in organic iodine production (Simondi-Teisseire et al., 2013).

The role of silver, originating from silver-indium-cadmium control rods, was highlighted in the Phébus-FP experiments (Simondi-Teisseire et al., 2013). Silver will react with dissolved iodine species to form for example insoluble silver iodide (AgI). This will limit the formation volatile I_2 regardless the sump pH.

2.3.2 Gas phase chemistry and retention of iodine

Volatile iodine will be absorbed and desorbed from surfaces in the containment of which most are painted. A painted surface is a sink for I_2 and a source for volatile organic iodine. The radiation induces fast radiochemical reactions between iodine and the paints. This phenomenon was observed in Phébus-FP experiments by a formation of a small steady-state concentration of iodine not dependent on pool pH (U.S. NRC, 2013). Also the air radiolysis products react with I_2 to form iodine oxides that are aerosols (Bosland et al., 2011).

Minimizing the iodine concentration in the containment atmosphere is important to minimize the possible source term to the environment through leaks or if the containment pressure needs to be decreased by venting. Venting lines may include filters that are able to retain almost all aerosol particles but only a small part of I_2 and a negligible part of organic iodides (Clément et al., 2007).

3 ASTEC V2.1

ASTEC (Accident Source Term Evaluation Code) is jointly developed by French IRSN and German GRS since 1996. ASTEC consists of several modules illustrated in Figure 2 of which each simulates a certain reactor zone or set of physical phenomena. In January 2017 was released the first revision of the new ASTEC series i.e. ASTEC V2.1.1.0. The new series includes several changes compared to former V2.0 series (Catelard & Reinke, 2015).

The main advances in terms of the code general features are related to the in-vessel coupling technique between the module dealing with thermalhydraulics of reactor coolant circuit (CESAR) and the core degradation module (ICARE). The new version also includes new models for core degradation addressing especially BWRs, but also useful for spent fuel pool accident analyses. The treatment of fission product transport and chemistry has also been renewed by harmonizing the modelling between the circuit and the containment in order to have a more consistent behaviour.

In addition to these general features, several modelling improvements have been made. Efforts have been focused on the reflooding of severely damaged cores, Zircaloy oxidation under air atmosphere, corium coolability aspects during Molten Core Concrete Interaction (MCCI) and gas phase chemistry kinetics in reactor coolant circuit. In addition, the modelling of iodine chemistry in the containment was improved according to recently achieved better understanding of gaseous iodine formation processes.

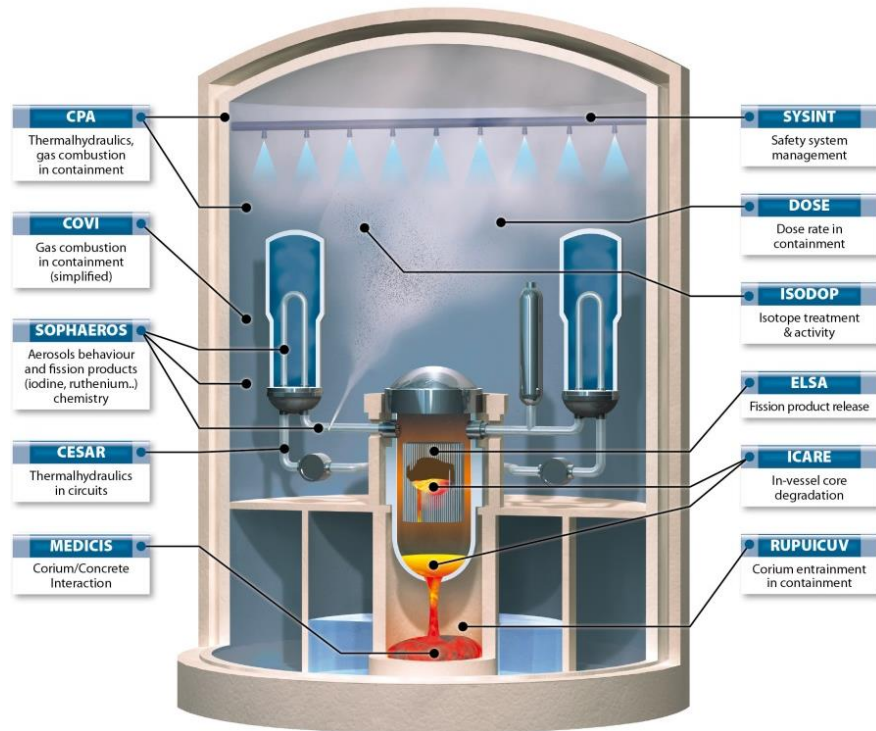


Figure 2. Scheme of ASTEC integral code.

3.1 SOPHAEROS module

In ASTEC V2.1 SOPHAEROS module is responsible for transport and chemistry of fission product vapours and aerosols in the reactor coolant circuit as well as in the containment. In previous version, CPA (Containment Part of ASTEC) module simulated aerosol physics in the containment and IODE module was responsible for iodine and ruthenium chemistry in the containment.

In vapour phase, SOPHAEROS takes into account the following phenomena:

- Gas equilibrium chemistry;
- Chemisorption of vapours on walls;
- Homogeneous and heterogeneous nucleation;
- Condensation and revaporisation on or from aerosols and walls;
- Kinetics of gaseous phase chemistry.

For aerosols, the following phenomena are analysed:

- Agglomeration: gravitational, Brownian diffusion, turbulent diffusion;
- Deposition mechanisms: Brownian diffusion, turbulent diffusion, eddy impaction, sedimentation, thermophoresis, diffusiophoresis, impaction in bends and deposit of aerosols in flow contraction;
- Remobilization of deposits: revaporisation and mechanical resuspension;
- Pool scrubbing.

Iodine and ruthenium chemistry in the containment covers about 50 possible chemical reactions that are the most predominant ones. The main modelled phenomena for mass transfer reactions are:

- Adsorption and desorption of molecular iodine on painted, metal and concrete walls;
- Mass transfer between sump and gas phase for diffusion or convection processes;

- Condensation of steam on the walls and on the sump surface;
- Transfer of non-volatile iodine oxides towards the sump;
- Effect of spray on molecular iodine: mass transfer between gas phase and droplet, interfacial equilibrium at the droplet surface, liquid mass transfers inside the droplet, chemical reactions in the bulk liquid.

Liquid phase chemistry includes:

- Hydrolysis of molecular iodine I_2 ;
- HOI dissociation/disproportionation;
- Oxidation of I^- by the oxygen dissolved in the sump water;
- Radiolytic oxidation of I^- into I_2 in the sump, where oxidation depends on the production rate of OH radicals, and where I_2 reduction is temperature-, pH- and $[I^-]$ -dependent;
- Reduction of iodates by radiolysis into molecular iodine;
- Silver iodide (AgI) formation by heterogeneous reactions (both Ag_2O/I^- and Ag/I_2 reactions are considered, the reaction of Ag_2O with I^- depends on the solubility of Ag_2O and AgI);
- Formation of organic iodide RI by homogeneous reaction in the liquid phase: solvents are released from paint in liquid phase, then oxidized under radiation to form organic acids and finally RI is formed by interaction between I_2 and solvents or sub-products;
- Decomposition of organic iodides in the liquid phase, according to two possible destruction processes radiolysis or hydrolysis.

In gas phase is modelled:

- Kinetics of air radiolytic products formation (represented by O_3);
- Oxidation of molecular iodine into iodine oxides (represented by I_2O_5) by air radiolysis products;
- Decomposition of iodine oxides into molecular iodine;
- Organic iodide formation from paints;
- Gas phase radiolytic destruction of organic iodide;
- Reaction between gaseous organics (CH_3R) and I_2 that can lead to the formation of gaseous organic iodide (methyl iodide (CH_3I)) is assumed to represent all the organic forms);
- Radiolytic decomposition of iodine oxides and multi-component aerosols into I_2 .

3.2 DOSE and ISODOP modules

The DOSE module (Cantrel, 2009) computes the dose rate in the containment gaseous phase with fission product distribution provided by SOPHAEROS. DOSE module has to be coupled with ISODOP module (Cousin & Jacq, 2015) that simulates decay of fission products and actinides. It starts the calculation using an initial isotope inventory given by the user.

ISODOP utilizes a dedicated data base containing the parameters for the radioactive decay between the isotopes. As an output isotope and element masses are produced at the end of each time step as well as α , β and γ powers and activity by mass of an element.

DOSE module utilizes ISODOP and SOPHAEROS output providing dose rates for bulk gas phase $D_{i,g}$ for each zone. The dose rate is calculated using formula 1:

$$\begin{aligned}
 D_{i,g} \text{ (Gy/s)} = & A_{i,w} \left[\underbrace{\frac{E_{i,\beta} \times k_2}{\rho V} \left(1 - \exp^{-\mu_{i,air} \times R}\right)}_{\beta \text{ contribution}} + \underbrace{\frac{E_{i,\gamma} \times k_3}{S} \sum_{j=O,H,N} x_j \left(\frac{\mu_{en}}{\rho}\right)_{i,j}}_{\gamma \text{ contribution}} \right] \\
 & + A_{i,g} \left[\underbrace{\frac{E_{i,\beta}}{\rho V} \left(1 - \exp^{-\mu_{i,air} \times R}\right)}_{\beta \text{ contribution}} + \underbrace{\frac{E_{i,\gamma}}{4\pi R^2} \sum_{j=O,H,N} x_j \left(\frac{\mu_{en}}{\rho}\right)_{i,j}}_{\gamma \text{ contribution}} \right]
 \end{aligned} \tag{1}$$

Where $A_{i,w}$ is activity of isotope i deposited on walls (Bq), $E_{i,\beta}$ is energy due to β disintegration of isotope i (J), $E_{i,\gamma}$ is energy due to γ disintegration of isotope i (J), k_2 and k_3 are empirical coefficients both fixed to 0.5 by default, which means that half of the emitted photons are towards the gaseous phase of the zone, ρ is density of the zone atmosphere (kg/m^3), V is volume of the zone (m^3), $\mu_{i,air}$ is linear attenuation coefficient for β radiation in air ($1/\text{m}$), R is the corresponding radius of the zone whose volume is assimilated to be spherical (m), S is area of the walls (m^2), x_j is mass fraction of hydrogen (H), oxygen (O) and nitrogen (N), μ_{en}/ρ is mass energy attenuation coefficient (m^2/kg) for element j (O, H or N) and $A_{i,g}$ is the activity of the isotope i in the bulk gas phase (Bq).

DOSE provides dose rates also on walls. The radioactive aerosols deposited onto walls are the source of the dose rate. For each zone, the area of walls is summed and a mean dose rate $D_{i,w}$ is calculated for each isotope i using formula 2.

$$\begin{aligned}
 D_{i,w} \text{ (Gy/s)} = & A_{i,w} \left[\underbrace{\frac{E_{i,\beta}}{\rho V_{layer}} \left(1 - \exp^{-\mu_{i,air} \times 0.1}\right)}_{\beta \text{ contribution}} + \underbrace{\frac{k_1 \times E_{i,\gamma}}{S} \sum_{j=O,H,N} x_j \left(\frac{\mu_{en}}{\rho}\right)_{i,j}}_{\gamma \text{ contribution}} \right] + \\
 & \underbrace{A_{i,g,layer} \times \left(\frac{E_{i,\beta}}{\rho V_{layer}}\right) \times \left[\frac{1}{2} \left(1 - \exp^{-\mu_{i,air} \times 0.05}\right) + \frac{1}{2}\right]}_{\beta \text{ contribution of gas phase}}
 \end{aligned} \tag{2}$$

Where $A_{i,g,layer}$ is activity of isotope i in the bulk layer gas phase (Bq), V_{layer} is volume of the layer around walls (m^3) of which thickness is fixed to 0.1 m and k_1 is empirical coefficient fixed to 0.3 by default.

4 NRC method for defining the dose rate

NRC (Nuclear Regulatory Commission) has introduced a method for defining dose rates in the air and water volumes (NRC, 1972). The method requires information on the spreading of the radioactive material in different volumes of the containment. Fission product distribution can be produced with an integral code like ASTEC or MELCOR. In integral codes fission products are dealt as elements, as in the case of ASTEC SOPHAEROS module, or even as a group of elements having similar chemical characters as in MELCOR. To have then the isotope distribution can be utilized for example ORIGEN2 (Gauld et al., 2011) that produces the isotope inventory for the whole core as a function of time from the shutdown.

4.1 Dose rate in the gas phase

Beta dose in the room gas phase is calculated using “Infinite Cloud” assumptions, i.e., the dimensions of the contaminated gas phase are assumed to be large compared to the distances that the beta particles travel (NRC, 1972). For an infinite uniform cloud, the beta dose rate in gas phase is:

$$D_{\beta,i} = 0.457 \cdot X_i \cdot E_{\beta,i} \quad (3)$$

, where $D_{\beta,i}$ is the beta dose rate from an infinite cloud, nuclide i (rad/s), X_i is the concentration of beta emitting isotope i in the room gas phase (curie/m³) and $E_{\beta,i}$ is the average beta energy of nuclide i per disintegration (MeV/dis).

For gamma emitting material, the dose rate in the room gas phase is (NRC, 1972):

$$D_{\gamma,i} = 0.507 \cdot X_i \cdot E_{\gamma,i} \cdot (1/G) \quad (4)$$

, where $D_{\gamma,i}$ is the gamma dose rate from an infinite cloud, nuclide i (rad/s), X_i is the concentration of gamma emitting isotope i in the room gas phase (curie/m³), $E_{\gamma,i}$ is the average gamma energy of nuclide i per disintegration (MeV/dis), G is a geometry correction factor.

The geometry correction factor addresses the fact that the containment room gas volume is a limited volume and it is thus inappropriately conservative to assume an infinite cloud of activity. The geometry correction factor is the ratio of the effective dose from an infinite cloud of activity to the effective dose from a finite cloud of activity and is calculated as (Murphy et al., 1974):

$$G = 351.6/V^{0.338} \quad (5)$$

, where V is the gas volume (m³). The averaged beta and gamma energies of the isotopes can be found in (Eckerman et al., 1993).

4.2 Dose rate in water

Assuming that radioactive material is uniformly distributed in the water pool both beta and gamma radiation dosage in the ambient water can be obtained. Beta particles have mean free paths less than 1 cm, therefore it can be concluded that all beta energy is absorbed in water. In the case of gamma radiation due to longer travel significant energy may escape absorption by water. Absorbed doses to water pools in severe accident sequences have been studied in (Weber, 1991). The average energy absorbed in water from γ decay is

$$E_{\gamma} = A + B \left(\frac{S}{V} \right) \quad (6)$$

, where E_{γ} is the average energy (MeV), A is a nuclide specific constant, B is a nuclide specific constant, S is the surface area (m²) and V is the water volume (m³).

A correlation was developed linking absorbed dose to source energy and surface-to-volume ratio of the pool. Several rectangular pools were studied. These results are now assumed to be transferable to pools of any geometry meaning that the only geometrical factor affecting energy absorption is the surface-to-volume ratio. Absorbed dose per unit mass of nuclide from beta and gamma radiation to water pool is calculated as:

$$d = 1.602 \cdot 10^{-11} \frac{(E_{\beta} + E_{\gamma}) \lambda N_a}{M m_{\text{wat}}}, \quad (7)$$

, where d is the specific dose rate due to electrons and photons (rad/s-g), E_{β} is the average energy (MeV) absorbed in water per β decay, E_{γ} is the average energy (MeV) absorbed in water per γ decay, λ is the nuclide decay constant (s^{-1}), N_a is the Avogadro's number, M is the atomic weight of nuclide and m_{wat} is the mass of water present (kg).

5 ASTEC input deck

For defining dose rates in a Nordic BWR containment, ASTEC input in which CPA, SOPHAEROS, DOSE and ISODOP modules were activated was utilized. Compared to the input deck used in previous analyses (Nieminen, 2016) the wet painted wall area was increased.

5.1 Containment and boundary conditions

A schematic figure of the ASTEC CPA module input is presented in Figure 3. The containment is modelled in four different compartments. Drywell (DRYW), wetwell (WETW), reactor cavity (CAVITY) and biological shield (SHIELD) next to the pressure vessel are defined as their own volumes.

There are several types of junctions available in ASTEC. The simplest one is the atmospheric junction to be defined between all volumes that are directly connected. This type of junction is defined from shield to drywell (SH_DW) and from drywell to cavity (A_DW_CA).

Since only gases are able to flow through atmospheric junctions, there need to be defined additional junction for drainage of water through an opening in the bottom of a volume. This is the case for flow from shield to cavity (atmospheric junction A_SH_CA and drainage junction D_SH_CA) and also for the flow from drywell to cavity (D_DW_CA).

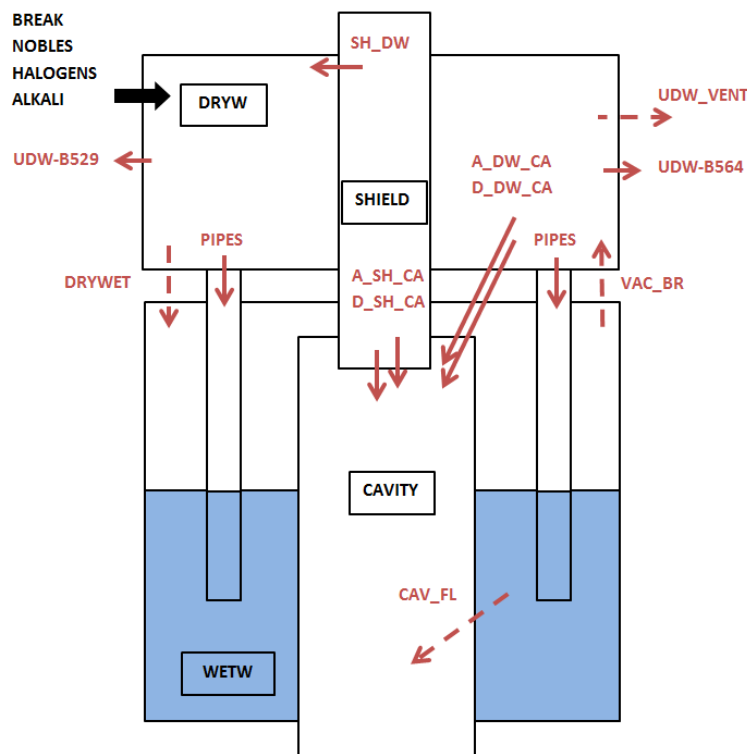


Figure 3. Schematic figure of the ASTEC input deck.

Also leakages from drywell to reactor building volumes are defined as simple atmospheric junctions (UDW-B529 and UDW-B564) but in this case they are directed directly to the environment since no reactor building volumes are modelled.

There exist a total of 16 blowdown pipes in the Nordic BWR containment included in a junction PIPES. These junctions are defined with a certain model used especially for vent pipes that take into account the pool scrubbing phenomenon. The rest of the junctions include some functions (marked with dashed line in Figure 3).

In order to ensure the coolability of the core melt after the release from pressure vessel, the containment cavity is flooded through a line from wetwell to cavity. This line (CAV_FL in Figure 3) is set to open at 1 800 s after the scram i.e. from the initiation of the calculation. Once opened the line remains open. However, it is set that a certain mass of water needs to remain in the wetwell pool.

Containment pressure is controlled by rupture disk venting (UDW_VENT). This line will be opened when the drywell pressure is 4 bars above the environment pressure if the drywell gas temperature is above 180 °C, and at 5 bars above the environment pressure below the temperature limit. Once opened the line will remain open, if no controller actions are done, decreasing the pressure effectively.

In addition to leaks from drywell to the reactor building, there is also a leak between the drywell and wetwell. The size of this leak is dependent from the drywell pressure. The leak is initially 0.0005 m², but when the drywell pressure increases from 5 bar to 5.1 bar, the leak increases linearly to 0.07 m². There exists also additional rule that if pressure at any point is above 5 bar, the leak size is from that point on at least 0.01 m². At 7.4 bars the leak size is set to 0.11 m². In ASTEC input the drywell-wetwell leak (DRYWET) flow path is set to increase from 0.0005 m² to 0.01 m² when the drywell pressure increases for the first time to 5.0 bar. After that the increase or decrease of the leak area is set to change stepwise as shown in Figure 4.

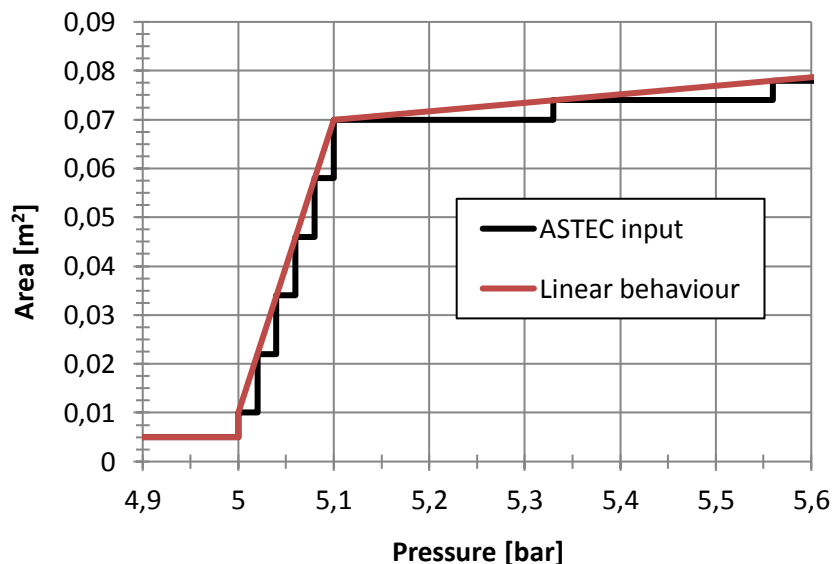


Figure 4. Drywell-wetwell leak size as a function of drywell pressure.

Between drywell and wetwell there is also a vacuum break line which will open if the wetwell pressure increases above drywell pressure more than 0.01 bar. The size varies as a function of pressure difference and the vacuum break line is fully open when the wetwell pressure is 0.1 bar above the drywell pressure. In ASTEC input the vacuum break line (VAC_BR) is actually modelled as a FAN structure to achieve correct behaviour

The mass flow of steam, water and hydrogen escaping from the primary circuit are all included into the same CONNECTION called BREAK. The TYPE of the SOURCE is FLUID. The values are taken from a MELCOR calculation output and corresponding values used in the ASTEC input can be seen in Figure 5 and in Figure 6.

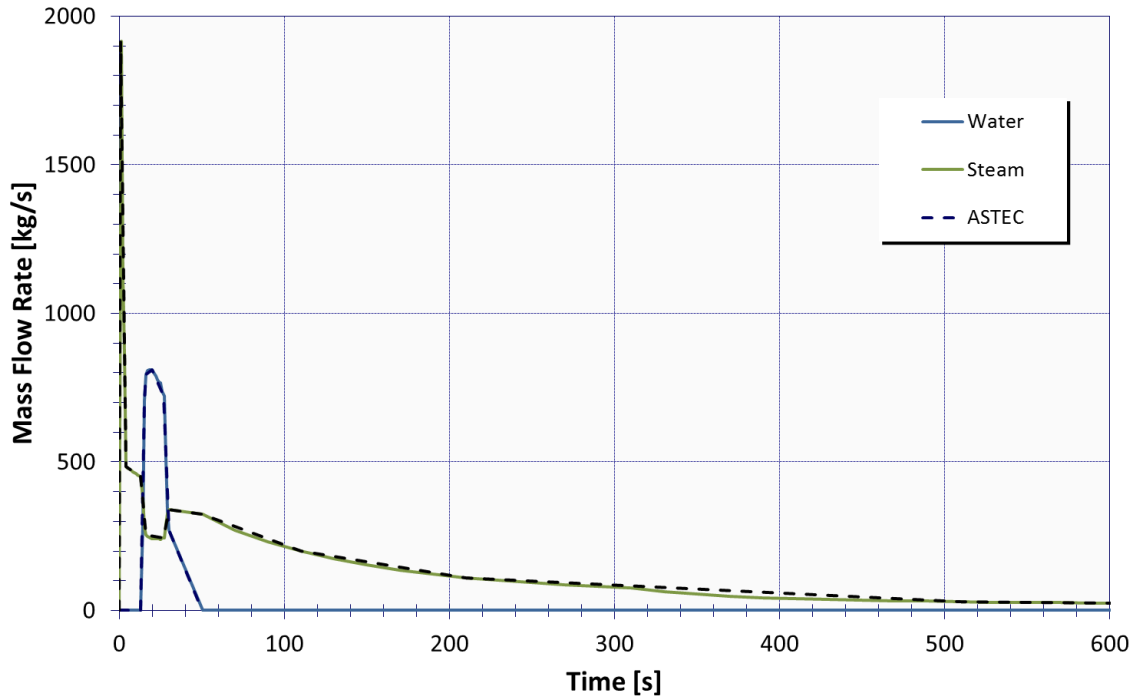


Figure 5. Mass flow of steam and water through the pipe break according to the reference MELCOR results and as entered to the ASTEC input.

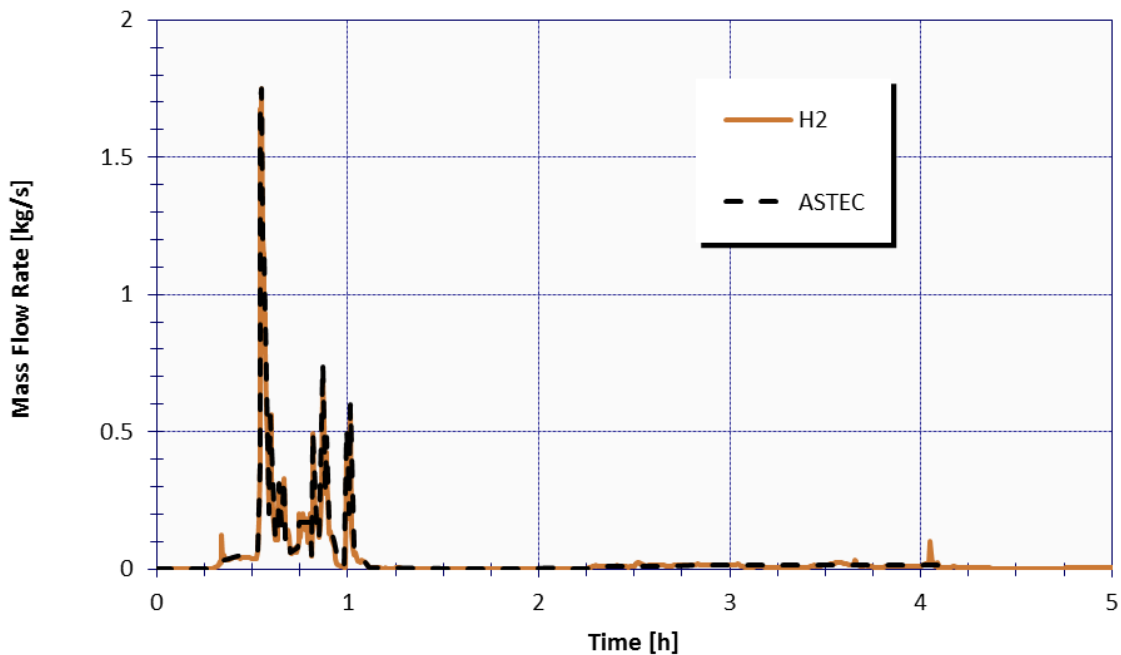


Figure 6. Mass flow of hydrogen through the pipe break according to the reference MELCOR results and as entered to the ASTEC input.

5.2 Fission product part

Initial isotope inventory was taken from OL1/OL2 FSAR report (Viitanen & Palomäki, 2011). Inventory calculations were originally made by (Lundgren, 2008). The inventory was calculated for a core thermal full power level of 2 500 MWt with an average discharge burn-up of 50 MWd/kgU. In the FSAR document are presented core inventories of noble gases, halogens, caesium and strontium and some important actinides. The most short-lived nuclides have been left out.

The isotope inventory is used for defining the fission product input and by the ISODOP module. The fission product release was assumed to follow the rules presented in the NUREG-1465 report and collected in Table 1. The simulated accident scenario was assumed to proceed to the end of early in-vessel release and only release of noble gases, halogens and alkali metals was taken into account.

The masses of all isotopes of a certain element were summed and mass flows were defined based on release fractions and durations of the release phases. The fission product input is illustrated in Table 2. The gap release was assumed to start 20 minutes after the initiating events of the postulated accident. All fission products were introduced to the code as elements and SOPHAEROS was responsible to define their chemical form after released in the containment. 5 % of iodine was assumed to be released in gaseous form and the rest as aerosols as well as all other elements.

Table 2. The fission product input.

		Total mass [kg]	Gap release [kg/s]	Early In-vessel release [kg/s]
1) Noble gases	Xe	0.753	2.0918E-05	1.3248E-04
	Kr	2.266	6.2941E-05	3.9863E-04
2) Halogens	I	14.656	4.0710E-04	6.7850E-04
	Br	0.001	2.6287E-08	4.3812E-08
3) Alkali metals	Cs	159.211	4.4225E-03	5.8967E-03
	Rb	0.001	2.6940E-08	3.5920E-08
Timing of the release:			20 min – 50 min	50 min – 2 h 20 min

6 Results

6.1 Thermal hydraulic behaviour

The pressure behaviour inside the containment can be seen in Figure 7. During normal operation the pressure is approximately 0.95 bar. Pressure increases rapidly in the containment after the pipe break and stabilizes at around 2.5 bar in the drywell and 1.8 bar in the wetwell. Pressure increase is controlled at this point with blowdown pipes. The steam mass flow through all 16 pipes can be seen in Figure 8.

Pressure starts to increase again when the fission product release to the containment begins at 20 min. Around the same time hydrogen production starts. Pressure decreases not until the drywell pressure reaches 5 bar and the rupture disk venting begins at around 3 h 54 min. The mass flow through the venting line is in Figure 9. At the same time, the drywell-wetwell leak increases to 0.01 m². The rupture venting decreases effectively the drywell pressure and the flow through the drywell-wetwell leak switches from wetwell to drywell only one minute after the rupture venting line has opened when the wetwell pressure becomes higher than the

drywell pressure. The mass flow through the leak is depicted in Figure 10 together with the leak size.

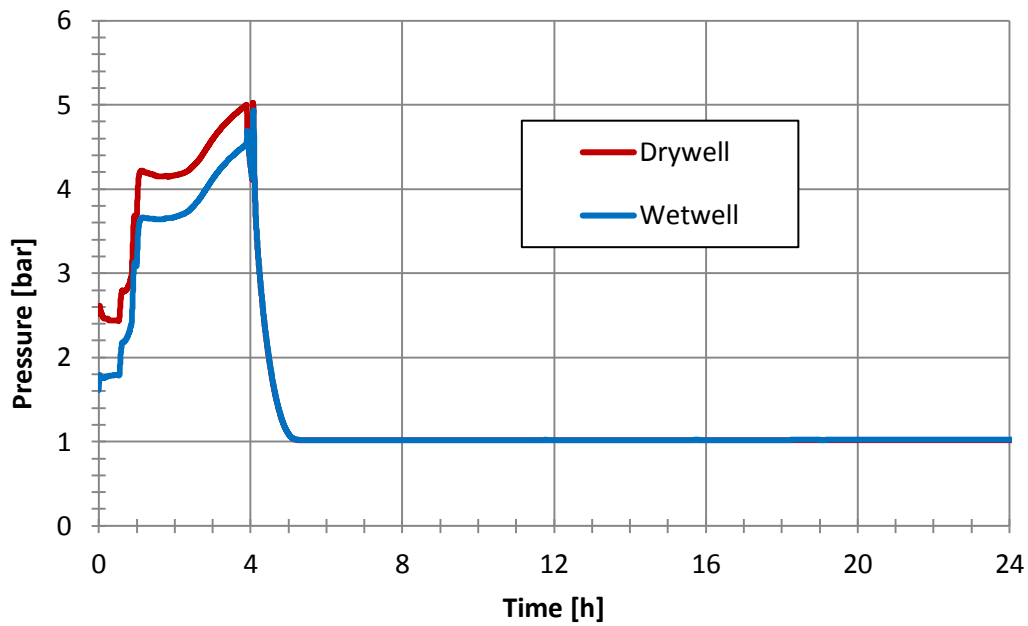


Figure 7. Pressure in the drywell and wetwell.

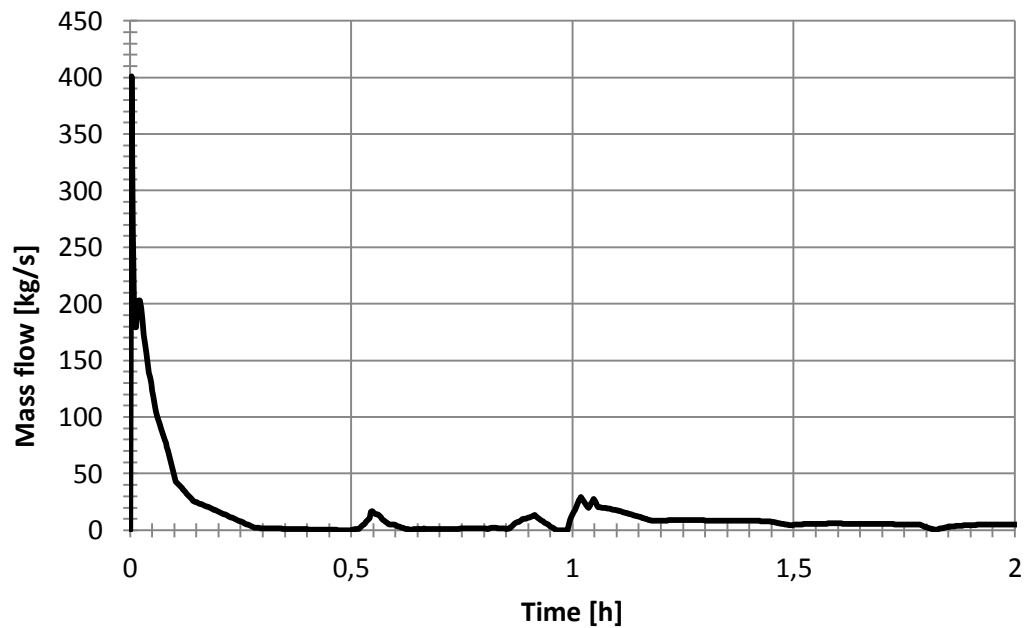


Figure 8. Total mass flow through the vent pipes.

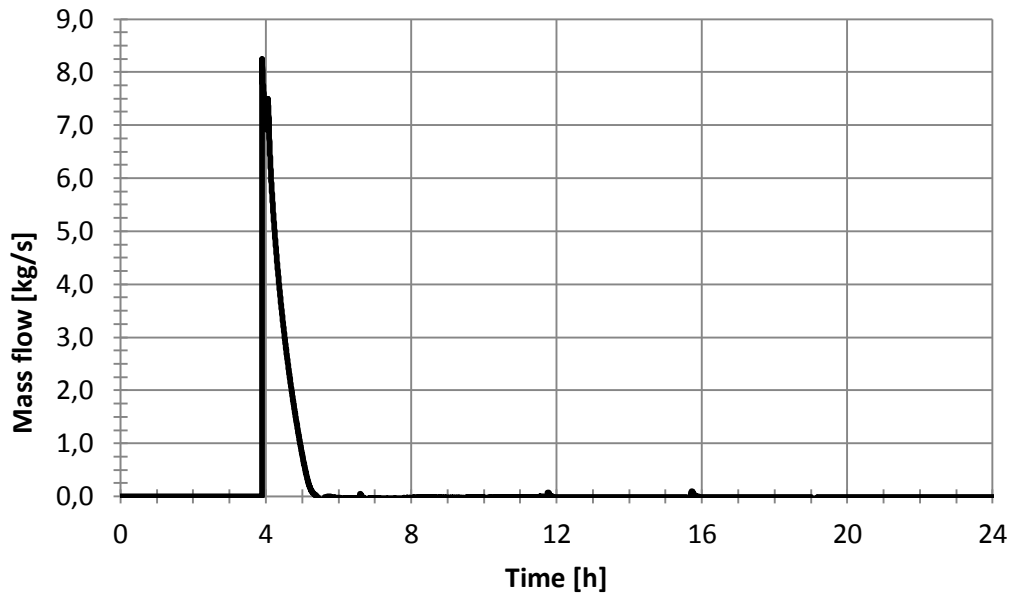


Figure 9. Mass flow through the rupture disk venting from drywell to decrease containment pressure.

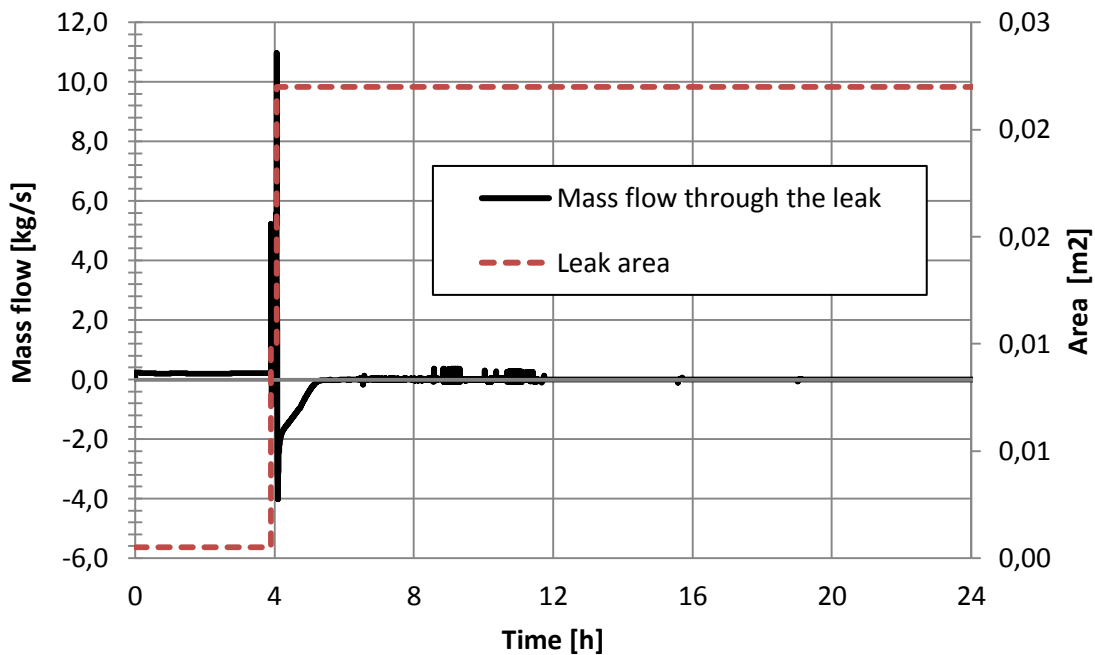


Figure 10. Mass flow through drywell-wetwell leak. Mass flow is positive when the flow is directed from drywell to wetwell.

Drywell-wetwell leak is not enough to balance the pressure difference between the compartments, and when the pressure in the wetwell becomes 0.01 bar higher than in the drywell, the vacuum breaker line (Figure 11) opens for the first time at around 3 h and 55 min and closes after 7 minutes. The line opens for the second time at 4 h 5 min closing after 39 min.

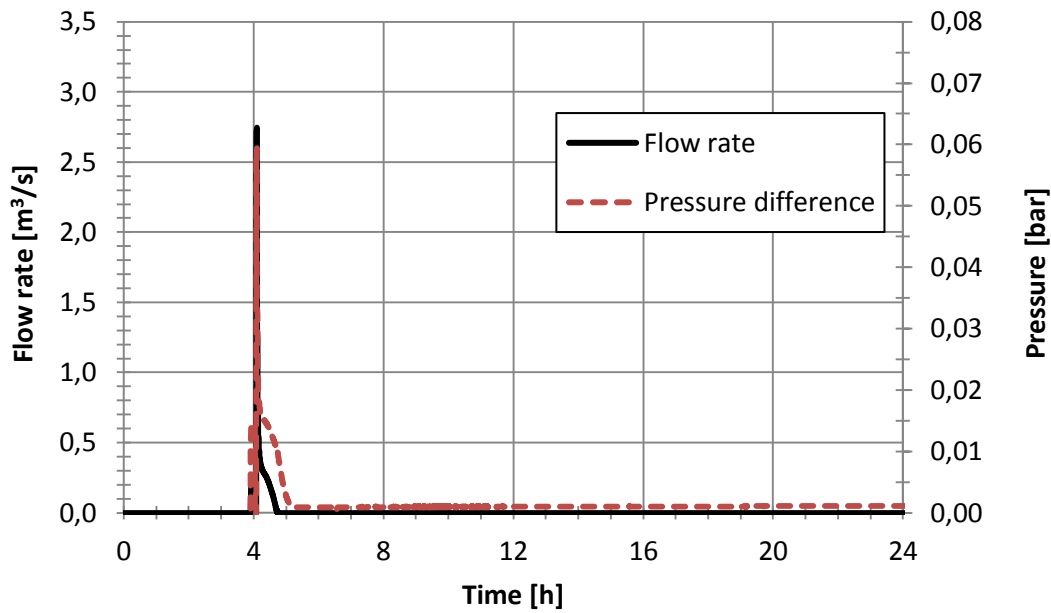


Figure 11. Mass flow through the vacuum breaker to equalize wetwell and drywell pressure when wetwell pressure is more than 0.01 bar higher.

Gas temperatures in the different compartments of the containment are depicted in Figure 12 as well as temperature of the wetwell pool. Decaying fission products heat the atmosphere. When the fission product input to the containment ends at 2h 20 min, the decay heat level in the containment is at its maximum, i.e. 2.38 MW. Based on simple formula $P = 0,125 P_0 t^{-0.28}$ the total decay heat level for a plant of which thermal power is 2 500 MW should be around 25 MW at that time. So nearly 10 % of the total decay heat is produced in the containment from that point on. The peak in the temperatures at 4 h 7 min is due to a sudden steam peak coming from the primary circuit to the containment heating the atmosphere and increasing the pressure. This is assumed to be caused by a small amount of debris slumping to the RPV lower plenum.

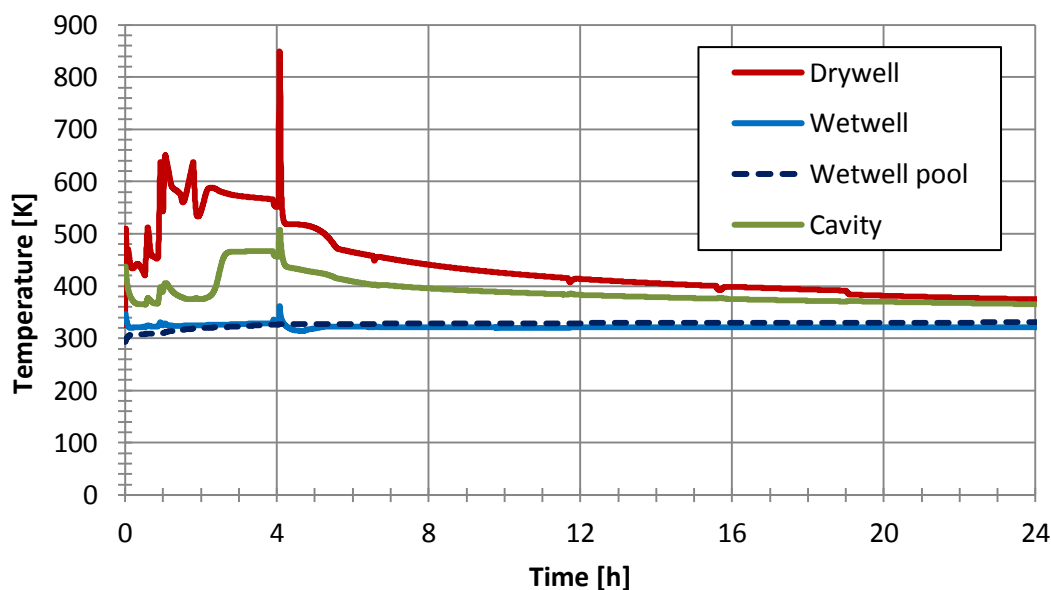


Figure 12. Gas temperatures in the containment and temperature of the wetwell pool.

6.2 The produced dose rates

Input data on fission product distribution for NRC method radiation dosage calculations was obtained from ASTEC output. SOPHAEROS module produces for each containment volume the total mass of each fission product element as well as deposited mass. For liquid phase is available the chemical compounds, based on which the mass of fission products can be calculated.

Defining dose rates with NRC method requires manual work so it was decided to determine them at 1 h, 3 h, 6 h, 12 h and 24 h and at those instances was defined also the elemental masses of Xe, Kr, I and Cs in gas phase and in water in each containment volume based on ASTEC results. To simplify calculations in this study the deposited fission products were included in the gas phase inventory. Then the isotope inventory at those instances was defined based on ORIGEN results and the dose rates calculated as presented in chapter 4. Contribution from the gas phase to water and vice versa was ignored in this work.

Dose rates in bulk gas phase in the different compartments of the containment are illustrated in Figure 13. According to ASTEC the dose rate in drywell gas phase has three local maximums: at 52 minutes the dose rate is 29.63 Gy/s, at 2 h 20 minutes it is 28.41 Gy/s and at 4 h 59 min it is 4.97 Gy/s. The dose rate in the cavity has two local maximums: at 2 h 31 min the dose rate is 13.27 Gy/s and at 5 h 7 min 5.57 Gy/s. Dose rate in the wetwell gas phase reaches its maximum value at 2 h 39 min being 2.09 Gy/s.

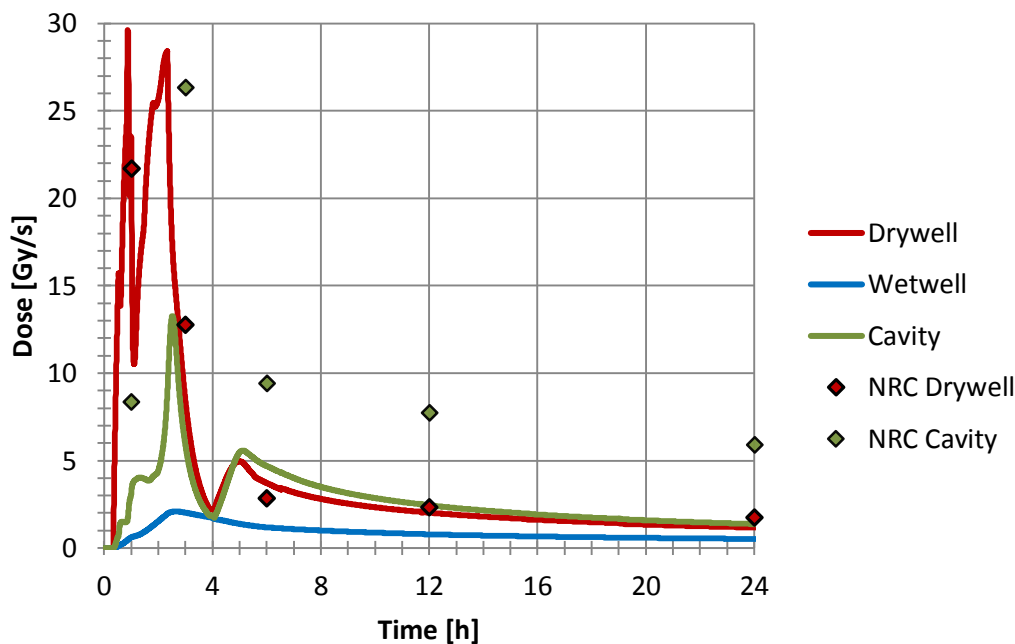


Figure 13. Dose rates in bulk gas phase.

The NRC method results are defined only for five time points so the dose peaks are difficult to observe reliably. As seen from Figure 13 the drywell gas phase dose rates produced with the different methods are nearly equal, but the cavity dose rates defined with NRC method are approximately twice the ASTEC dose rates.

In Figure 14 is presented separately the beta and gamma dose rates in drywell atmosphere defined with both methods. To simplify the comparison, only the corresponding time points of ASTEC results with NRC method are depicted. Beta dose rates are nearly equal but the gamma dose rates have larger difference especially at later time points. In Figure 15 can be

seen the data for cavity atmosphere. In this case also the beta dose differs notably and the gamma dose behaves more or less similarly as in drywell.

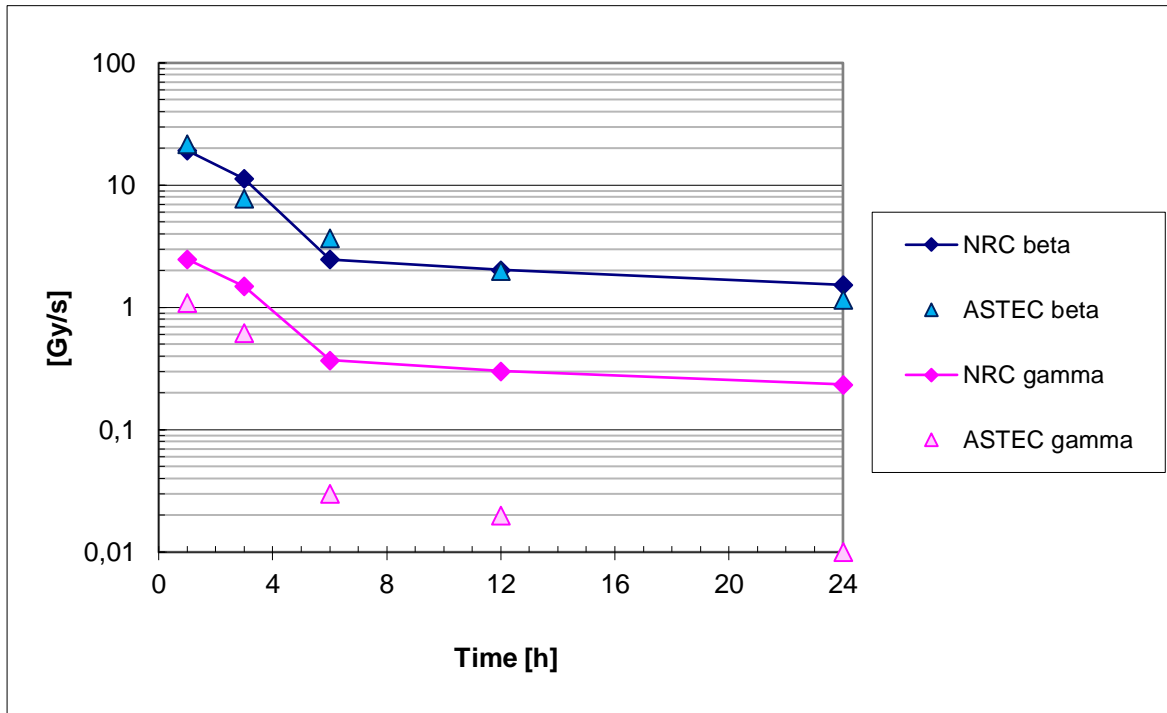


Figure 14. Dose rates produced by beta and gamma radiation in the drywell atmosphere according to ASTEC and NRC method.

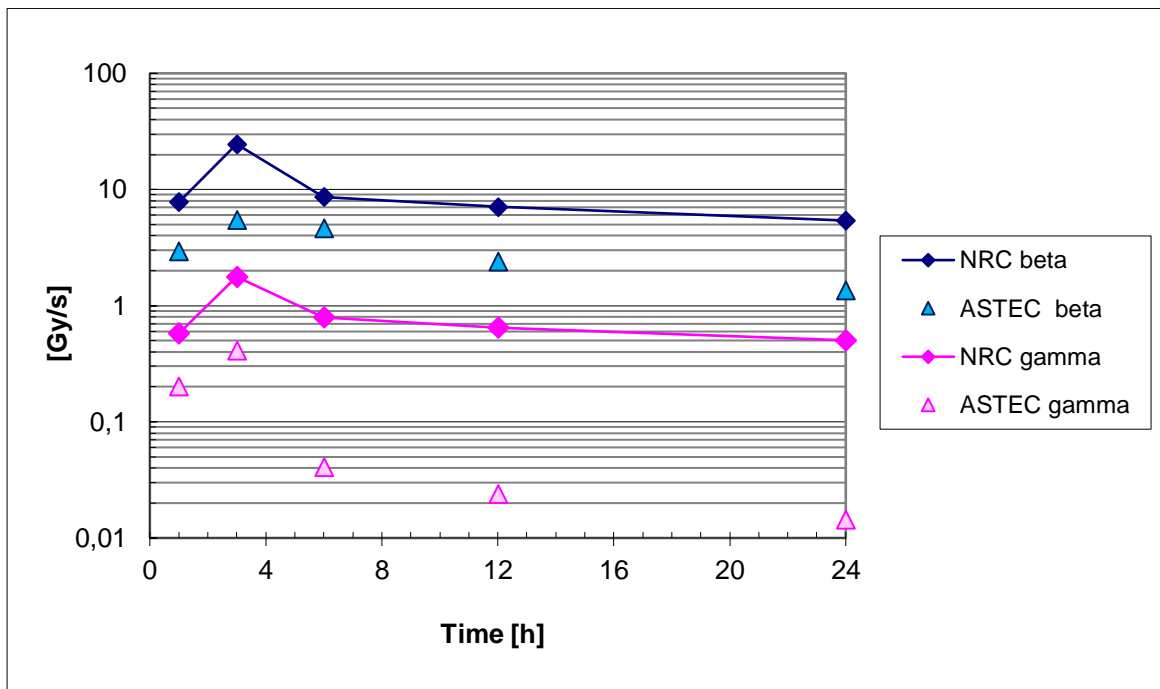


Figure 15. Dose rates produced by beta and gamma radiation in the cavity atmosphere according to ASTEC and NRC method. To simplify the comparison, only the corresponding time points of ASTEC results with NRC method are depicted.

Table 3. Fractions of dose rates produced by different elements in the drywell gas phase according to ASTEC results. TOT column tells what is the fraction of the total dose rate that is produced by the isotopes taken into account in NRC method calculation according to ASTEC.

Beta dose					
Time	Xe	Kr	I	Cs	TOT
1 h	0.17	0.23	0.36	0.10	0.86
3 h	0.34	0.20	0.36	0.02	0.93
6 h	0.18	0.04	0.69	0.04	0.96
12 h	0.24	0.02	0.68	0.06	0.99
24 h	0.29	0.00	0.62	0.09	1.00
Gamma dose					
Time	Xe	Kr	I	Cs	TOT
1 h	0.05	0.54	0.31	0.06	0.97
3 h	0.08	0.67	0.23	0.01	0.99
6 h	0.09	0.37	0.48	0.06	0.99
12 h	0.13	0.28	0.49	0.10	1.00
24 h	0.15	0.30	0.40	0.15	1.00

Table 4. Fractions of dose rates produced by different elements in the cavity gas phase according to ASTEC results. TOT column tells what is the fraction of the total dose rate that is produced by the isotopes taken into account in NRC method calculation according to ASTEC.

Beta dose					
Time	Xe	Kr	I	Cs	TOT
1 h	0.14	0.18	0.35	0.14	0.81
3 h	0.32	0.19	0.36	0.02	0.89
6 h	0.07	0.02	0.78	0.02	0.89
12 h	0.09	0.01	0.83	0.04	0.97
24 h	0.11	0.00	0.83	0.06	1.00
Gamma dose					
Time	Xe	Kr	I	Cs	TOT
1 h	0.05	0.44	0.38	0.09	0.96
3 h	0.08	0.63	0.27	0.01	0.99
6 h	0.03	0.11	0.79	0.05	0.98
12 h	0.03	0.07	0.80	0.08	0.99
24 h	0.04	0.08	0.73	0.14	0.99

In Table 3 are presented the fractions of total beta and gamma dose rates produced by different elements according to ASTEC results for the drywell gas phase and in Table 4 the corresponding data for the cavity gas phase. It can be concluded that in the long term, iodine is the most important dose producer and at early stage noble gases are dominating. Beta and gamma dose rates in the cavity and drywell gas phase produced by different isotopes based on ASTEC and NRC method results are depicted in Appendix A.

ASTEC produces also dose rates on inner walls that can be seen in Figure 16 for drywell and cavity. The dose rates on walls are notably higher than dose rates on gas phase due to the amount of deposited aerosols. In drywell the dose rate on wall reaches its maximum, i.e. 48.84 Gy/s at 5 h 7 min. In cavity the maximum dose rate is even higher, 91.02 Gy/s at 5 h 11 min, since the temperature is lower and therefore there are less gaseous fission products compared to aerosols and more deposited aerosols per wall area. In wetwell there is no dose rate on wall, since DOSE module produces no dose rate on wet wall.

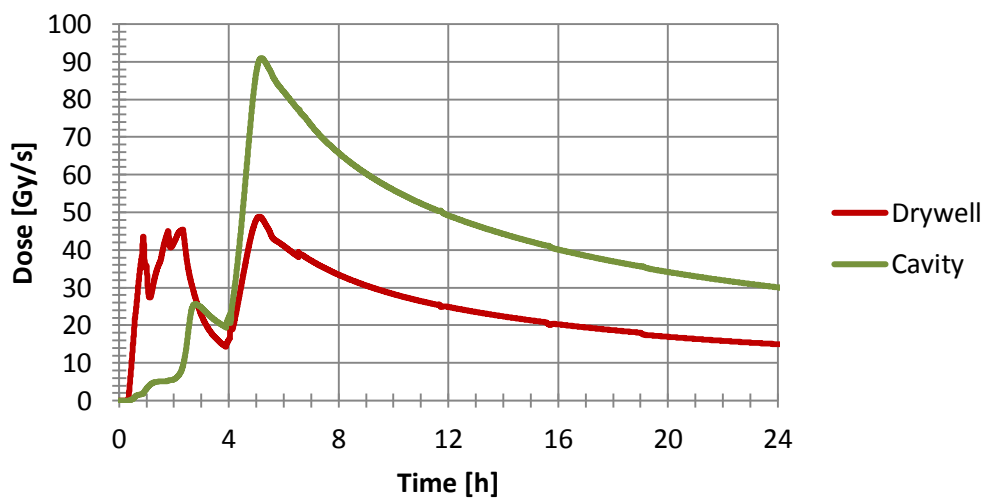


Figure 16. Dose rate on inner wall.

In Figure 17 are the dose rates in wetwell and cavity water produced by ASTEC and NRC method. In this case the values for cavity match better but the difference also in wetwell values can be considered rather small.

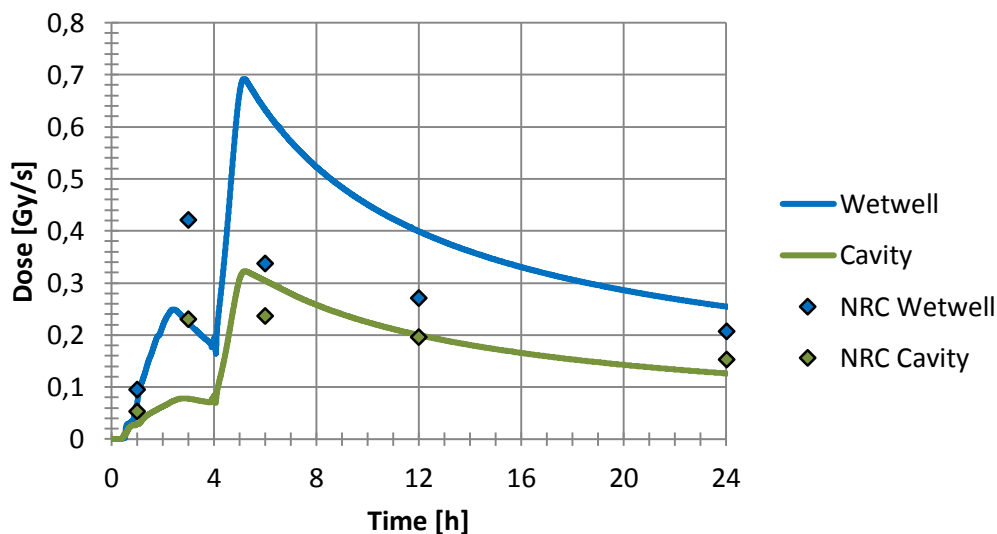


Figure 17. Dose rates in water.

6.3 Fission product behaviour

The behaviour of fission products explain the behaviour of dose rates. Masses of gaseous fission product compounds in the drywell are in Figure 18, in the wetwell in Figure 19 and in the cavity in Figure 20. Since temperatures remain rather low in wetwell gas space and also in cavity, only the noble gases and iodine are there in gaseous form. To the wetwell remains a constant inventory of noble gases after 5 h, since after that there is practically no pressure difference between drywell and wetwell and therefore there are no notable flows between these compartments. Gaseous fission products from drywell and cavity are more efficiently directed to the venturi scrubber in the rupture disk venting line. The size of the flow path between cavity and drywell is 1.9 m^2 whereas the drywell-wetwell leak is only 0.01 m^2 during the drywell venting.

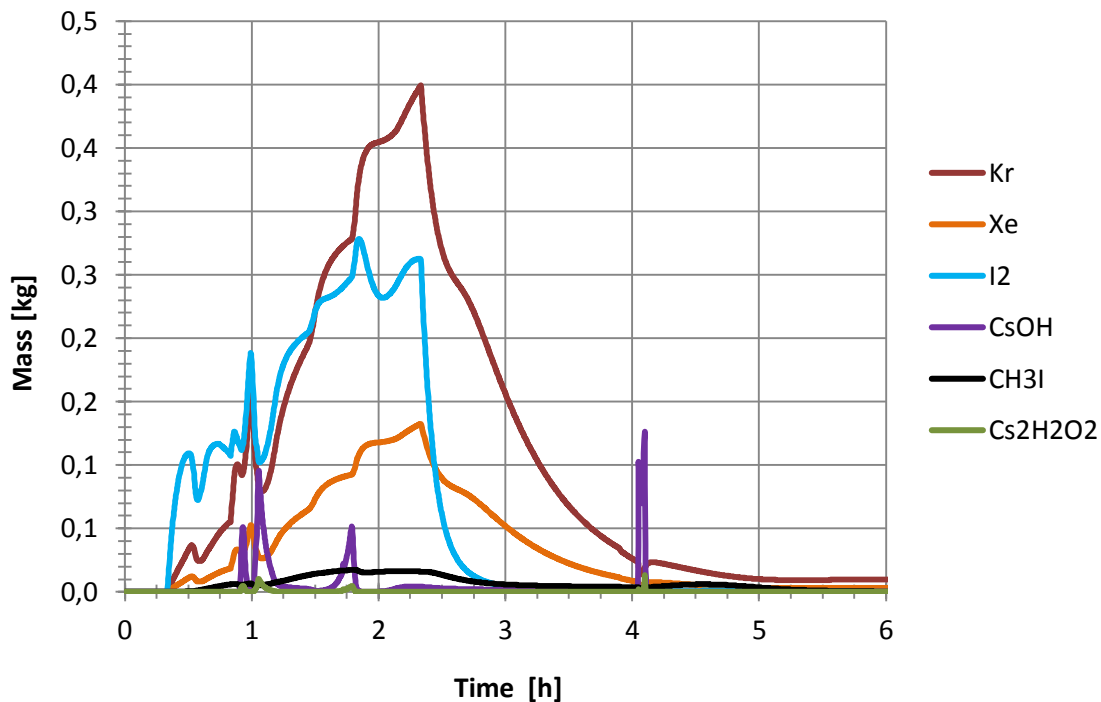


Figure 18. Gaseous fission products in the drywell.

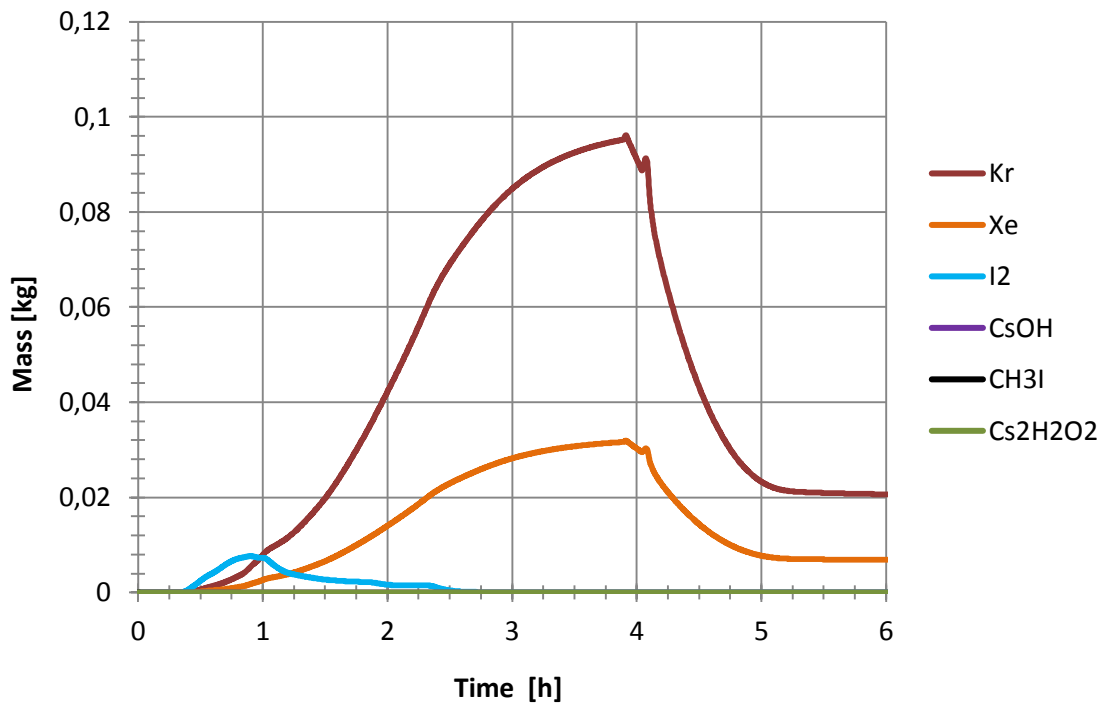


Figure 19. Gaseous fission products in the wetwell.

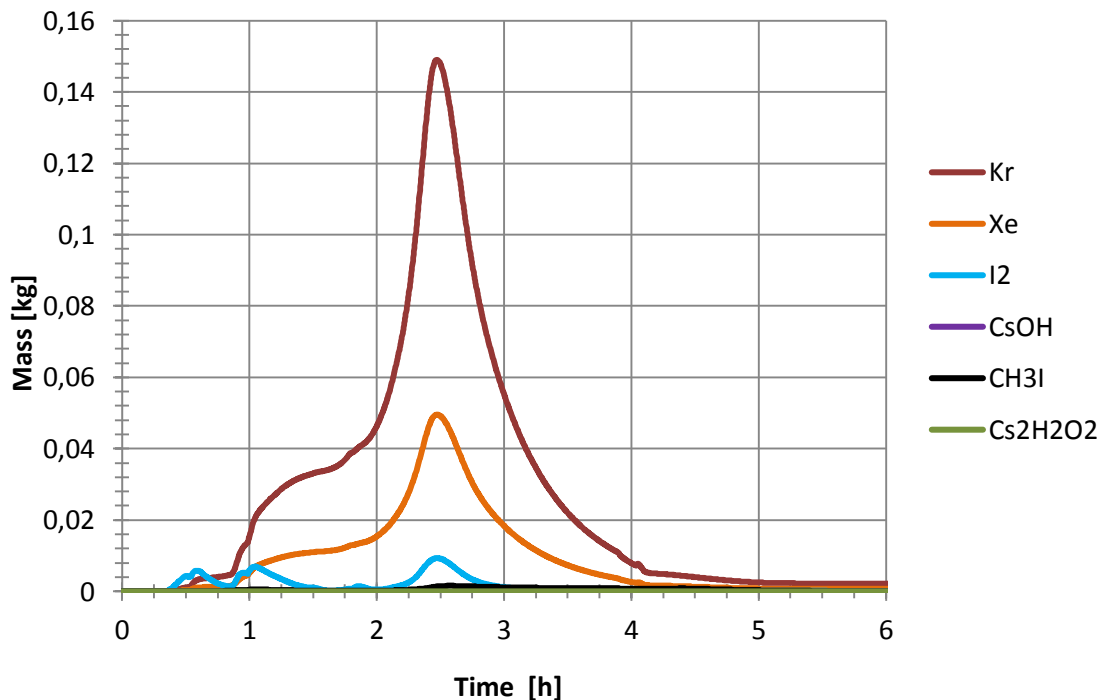


Figure 20. Gaseous fission products in the cavity.

Masses of airborne aerosol compounds in the drywell are in Figure 21, in the wetwell in Figure 22 and in the cavity in Figure 23. When neglecting the noble gases, more fission products are present in the containment in aerosol form. As is the case with noble gases, there also remains a constant inventory of aerosols to the wetwell atmosphere. In the drywell and in the cavity, all aerosols are either deposited or directed to the venturi scrubber.

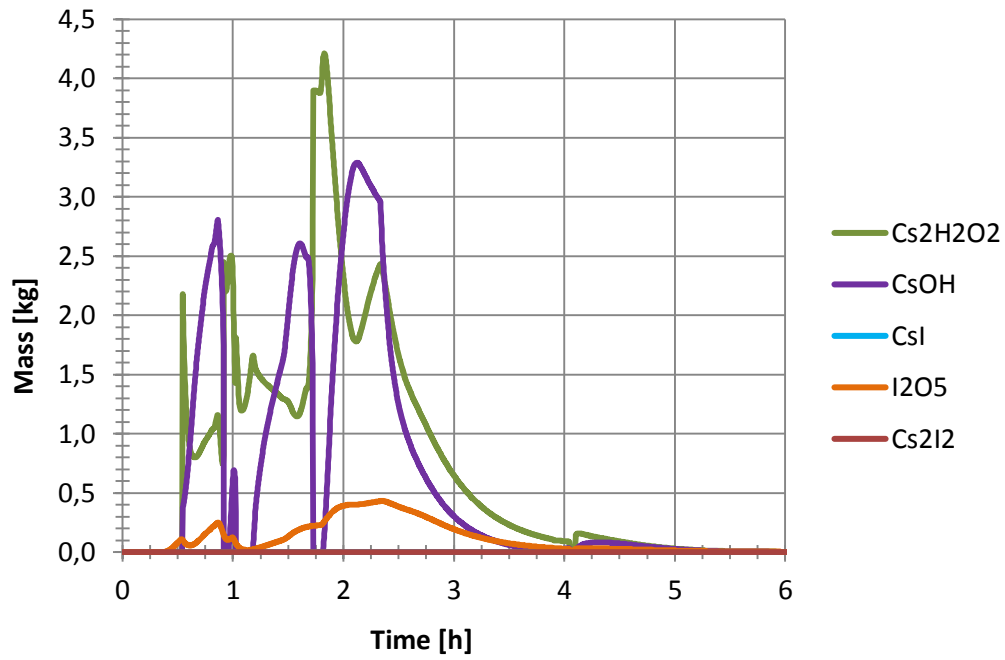


Figure 21. Aerosols in the drywell.

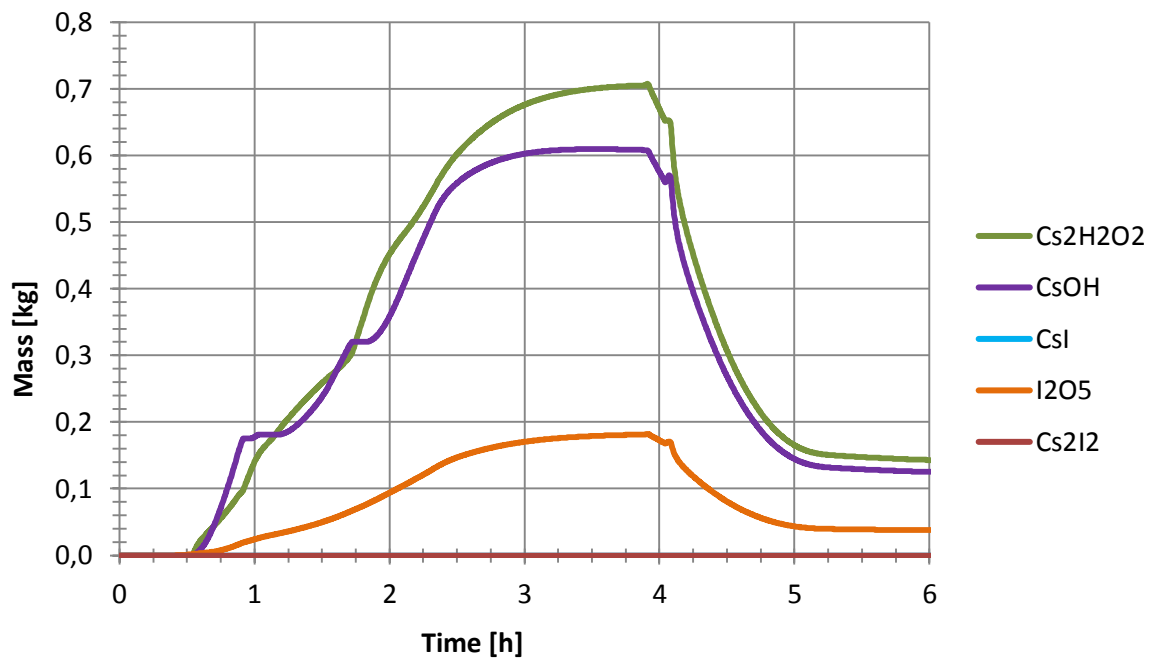


Figure 22. Aerosols in the wetwell.

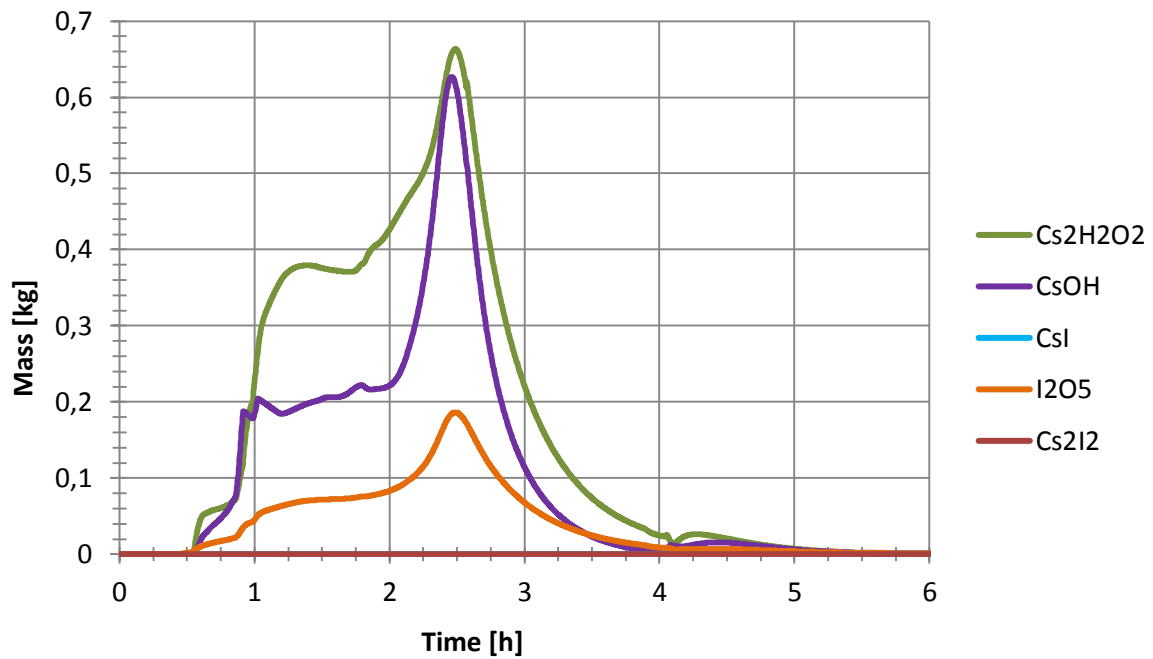


Figure 23. Aerosols in the cavity.

Aerosols deposit rather fast in the containment. The masses of deposited aerosols in the drywell are in Figure 24 and in the cavity in Figure 25. At 6 h 8.9 % of Cs and 6.7 % of I in the containment was deposited. In the end of the calculation 50.17 % of the deposited aerosols deposited by thermophoresis, 10.23 % by settling and 39.03 % by diffusiophoresis.

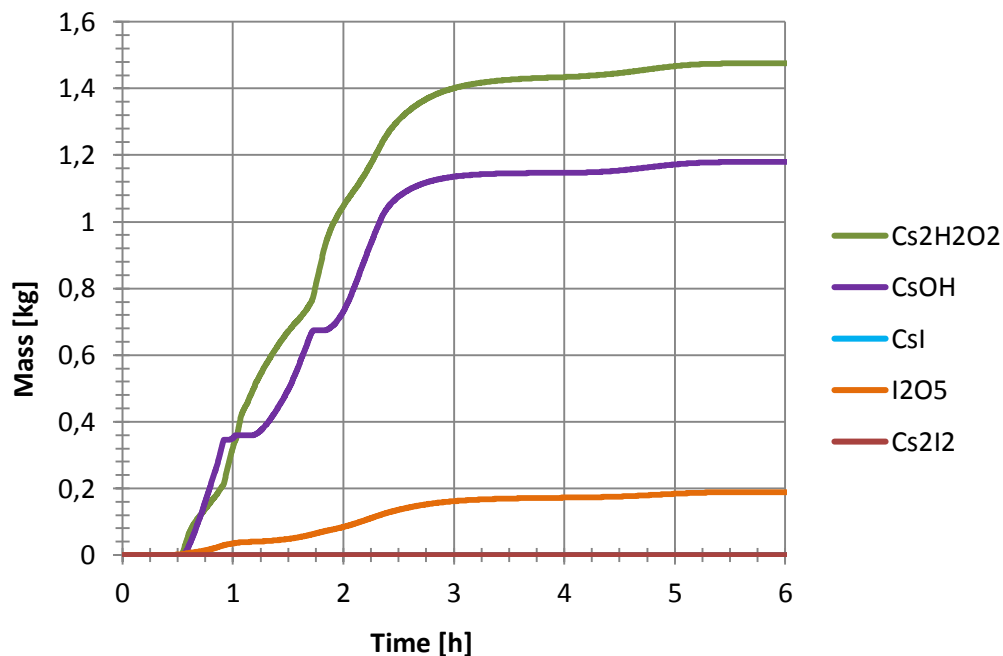


Figure 24. Deposited aerosols in the drywell.

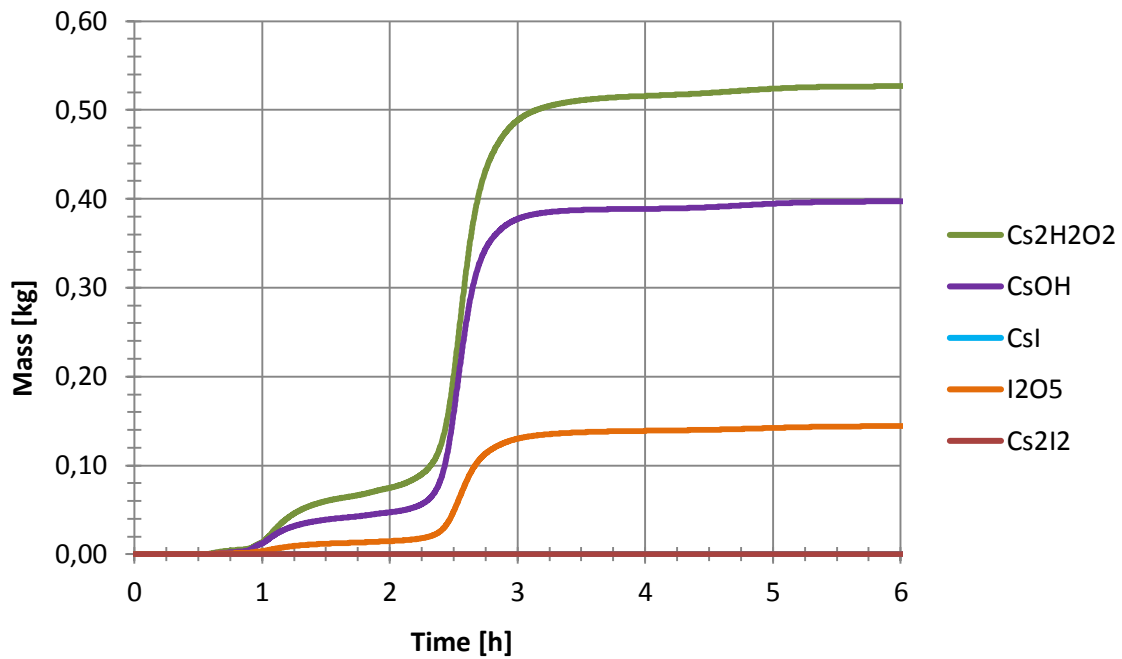


Figure 25. Deposited aerosols in the cavity.

In Figure 26 can be seen the masses of dissolved fission products in the wetwell pool and in Figure 27 in the cavity. The masses in the wetwell increase as long as there is some flow through the vent pipes (Figure 8). In the cavity, the increase continues until the water mass increases. Water depth in the wetwell and in cavity is illustrated in Figure 28. At 6 h 90.4 % of Cs, 92.4 % of I and 98.5 % of Xe and Kr were dissolved in water. Ph of the pools did remain at 5.0 which is the reference value in ASTEC.

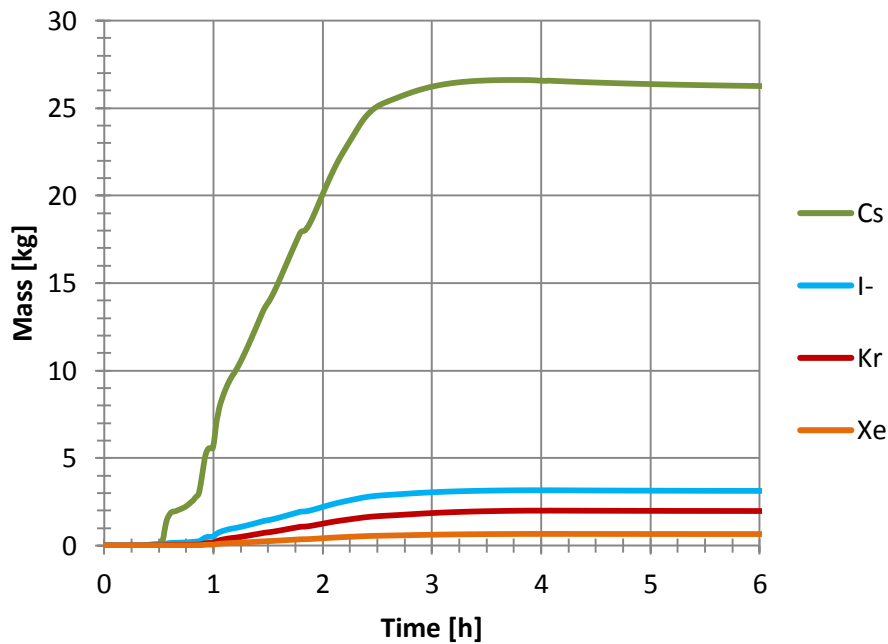


Figure 26. Fission products dissolved in water in the wetwell.

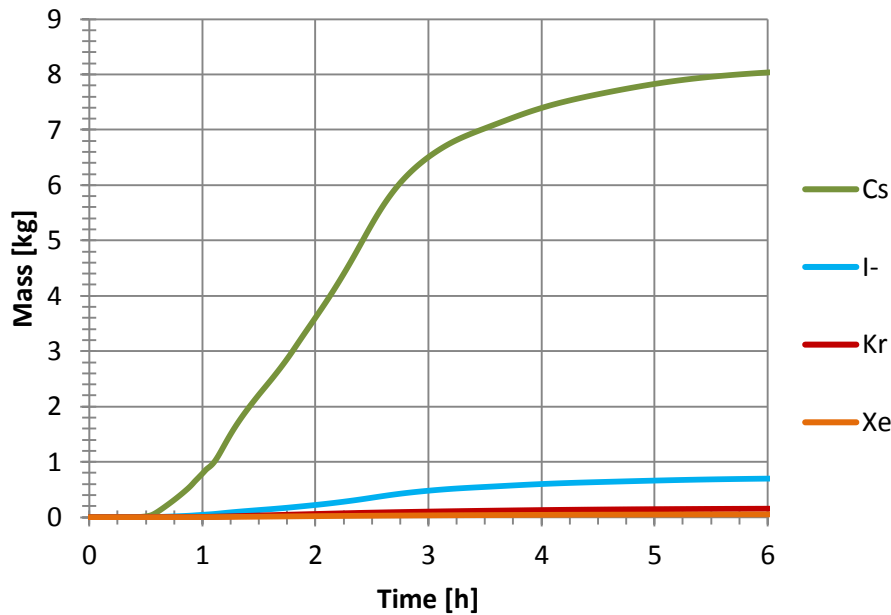


Figure 27. Fission products dissolved in water in the cavity.

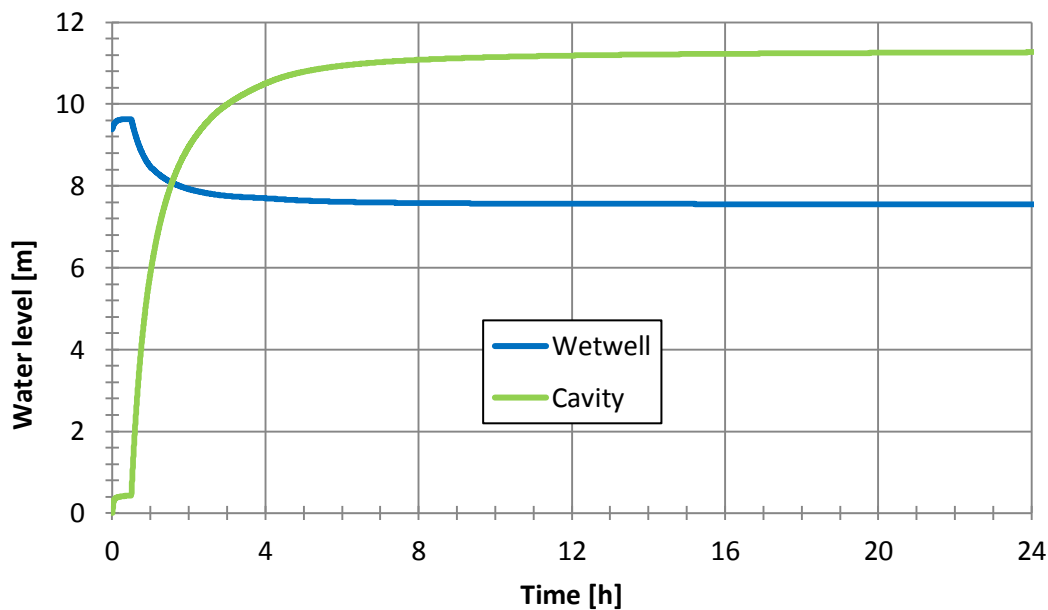


Figure 28. Water depth in the wetwell and in cavity.

6.3.1 Comparison to previous results

As mentioned before, compared to the previous ASTEC dose analyses the wet painted wall area was increased in the containment because it was clarified, that SOPHAEROS cannot change wall area that is initially defined to be dry to be wet. In the drywell the floor area was now defined to be wet and in the cavity the submerged wall area when the cavity is fully flooded was defined to be already initially wet. Previously was also assumed that the wetwell pool wall was steel, but now also that was assumed to be painted.

In Figure 29 is presented the iodine compounds in the drywell gas phase, in Figure 30 in the wetwell and in Figure 31 in the cavity. Dashed lines indicate the previous analysis results and solid lines the news ones. I_2 and CH_3I are gaseous compounds whereas CsI , Cs_2I_2 and I_2O_5

are present as aerosols. Gaseous iodine and iodine oxides are now the primary compounds instead of caesium bearing aerosols. In water was dissolved more fission products than before.

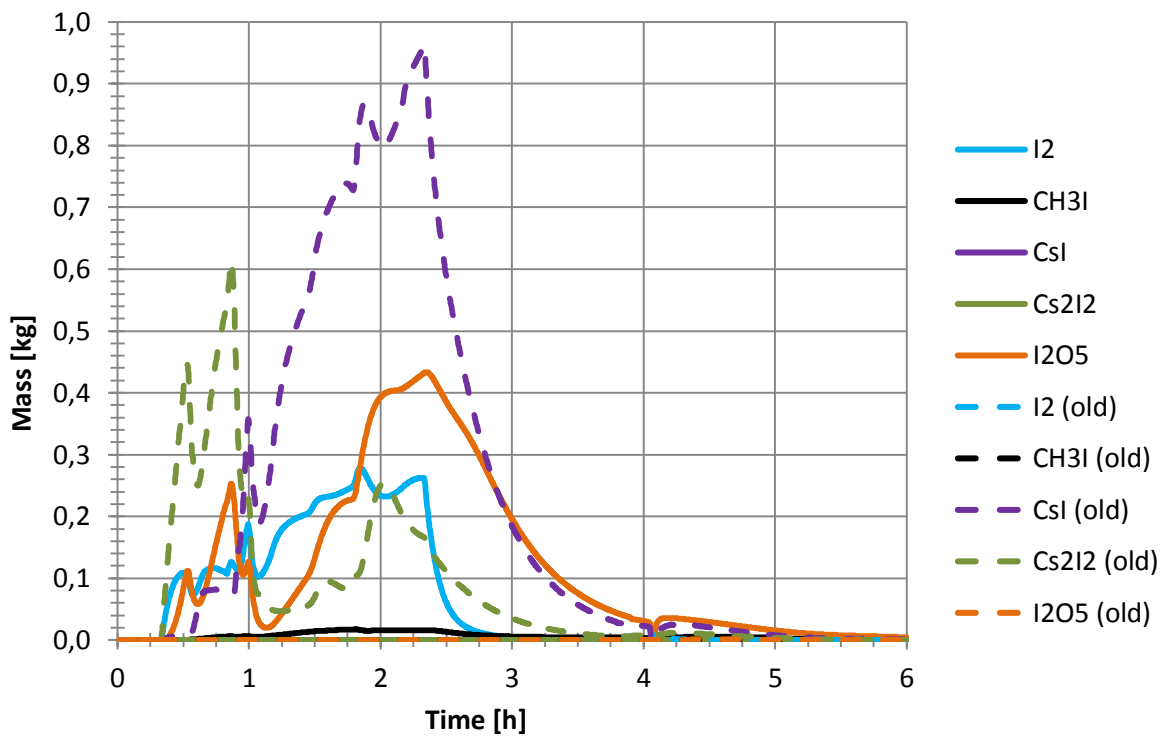


Figure 29. Iodine compounds in the drywell. Dashed lines indicate previous analysis results, where the area of wet painted wall was defined notably smaller.

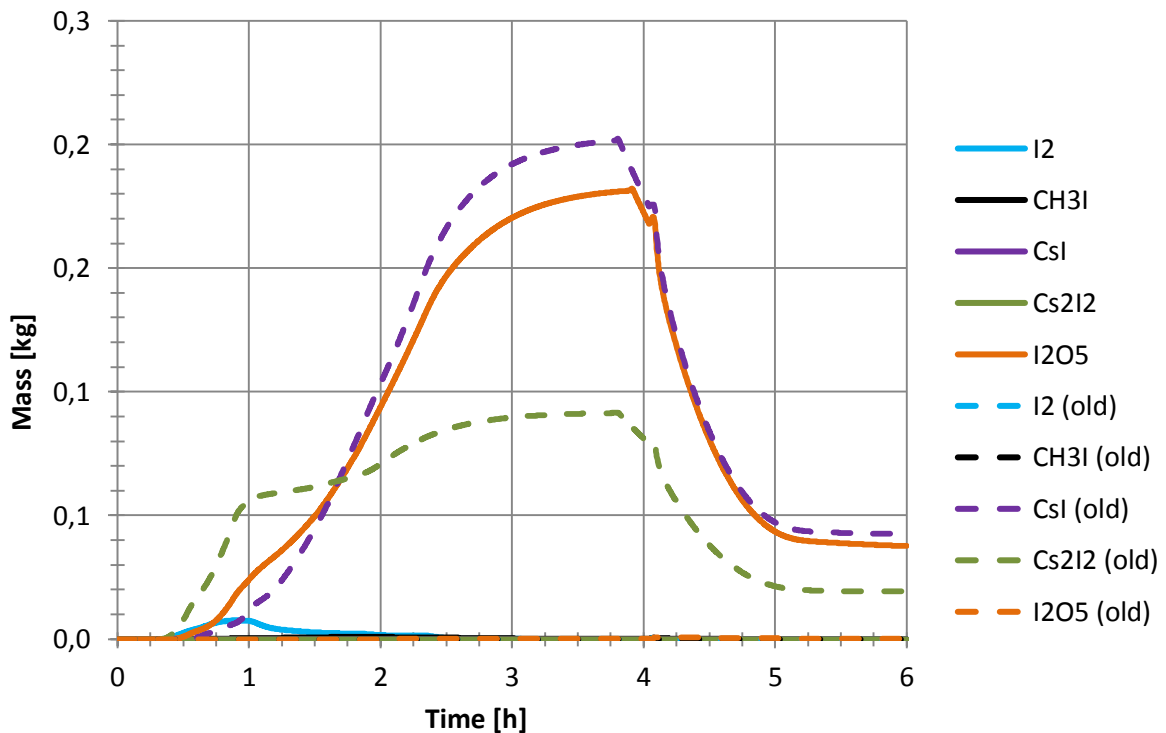


Figure 30. Iodine compounds in the wetwell. Dashed lines indicate previous analysis results, where the area of wet painted wall was defined notably smaller.

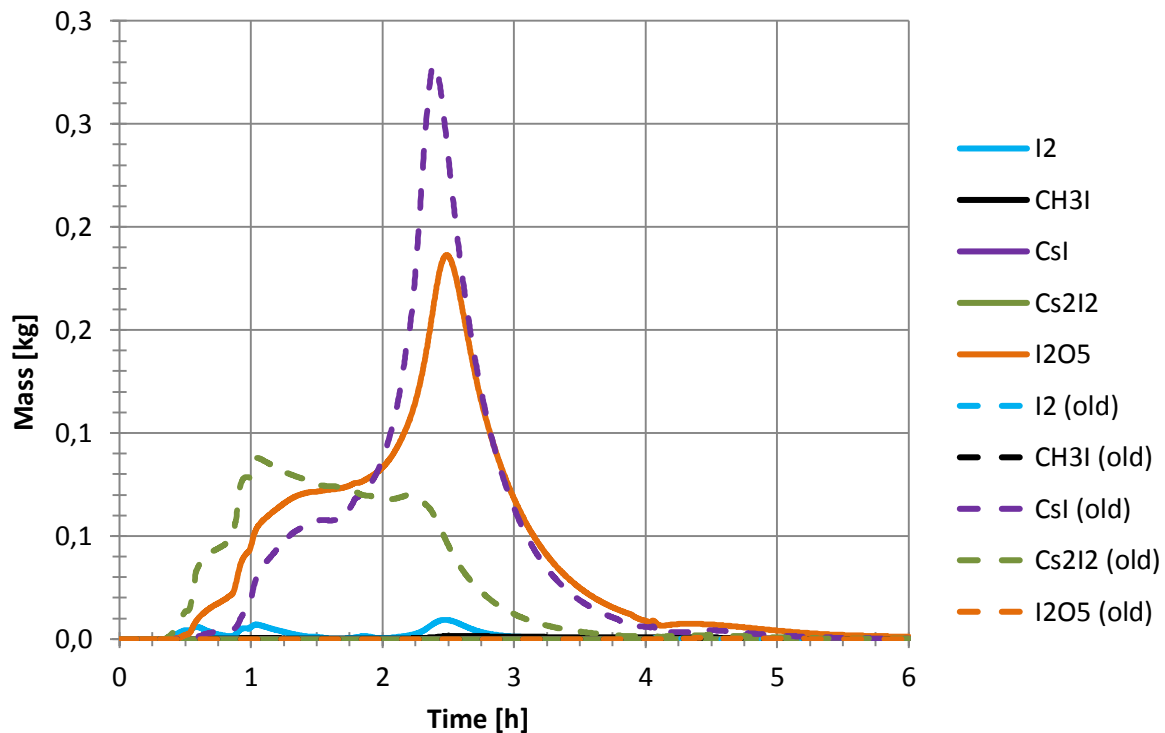


Figure 31. Iodine compounds in the cavity. Dashed lines indicate previous analysis results, where the area of wet painted wall was defined notably smaller.

7 Discussion and conclusions

The objective of this work was to compare the dose rates in containment produced by integral code ASTEC and by NRC method. The selected test case was a large LOCA in a Nordic BWR. The source term to the containment was defined based on NUREG-1465 report. Fission product distribution for NRC method dose calculations was obtained from ASTEC.

The basic assumption was that the dose rates produced by NRC method are higher than the ASTEC dose rates because the deposited fission products were included in the gas phase inventory and because ASTEC assumes that 50 % of the radiation from the deposited fission products is absorbed by the wall. This assumption is more or less confirmed, but the difference was higher than expected for all but drywell beta dose rate.

NRC beta dose rate in the cavity is nearly approximately twice the ASTEC dose rate in cavity atmosphere but in drywell they are more or less equal. In ASTEC the beta dose rate is inversely proportional to the volume of the zone. When the cavity is flooded the gas volume becomes approximately half smaller. If ASTEC DOSE module uses the initial volume of the zone, the difference is explained. The difference also becomes larger at later time points when the cavity gas volume becomes even smaller that supports the theory. However, in all cases the total dose rate estimates were within a factor of two that can be considered rather acceptable difference taking into account different approach in the methods.

In ASTEC dose rates, there is a peak after four hours despite the fission product inventory does not increase in any of the volumes as indicated in the figures of chapter 6.3. This peak is produced by iodine as observed from Appendix A figures. The fission product chemical and physical behaviour is calculated by SOPHAEROS module but the decay chains are dealt by ISODOP module. It is assumed that from the ISODOP point of view, iodine inventory is

increasing, but SOPHAEROS does not take into account this fission product change into other elements by decaying.

ASTEC input was also changed by increasing the wet painted wall area in the containment. It was expected that this would increase the mass of organic iodide, but it increased more notably the mass of I_2 and iodine oxides. This is assumed to result from organic iodides radiolytically destructing into I_2 and I_2 then reacting with air radiolysis products to form iodine oxides.

The change in iodine behaviour resulted slightly higher dose peaks in the containment gas phase but notably smaller dose rates on walls. In total 98.71 % of fission products were retained in the containment, which is 1.5 % more than in previous analysis. This is mostly because the amount of dissolved fission products is higher.

References

- Bosland, L., Funke, F., Girault, N. & Langrock, G. 2011. PARIS project: radiolytic oxidation of molecular iodine in containment during a nuclear reactor severe accident. Part 2: formation and destruction of iodine oxides compounds under irradiation – Experimental results modelling. *Nuclear Engineering and Design*. Volume 241. pp. 4026-4044.
- Cantrel, L. 2009. Description of the DOSE module of ASTEC V2. Rev.0. ASTEC-V2/DOC/09-14. Report DPAM/SEMIC 2009-357. 22 p.
- Chatelard, P. Belon S., Bosland, L., Carénini, L., Coindreau, O., Cousin., F., Marchetto C., Nowack H., Piar, L. & Ckailan L. 2015. Main modelling features of the ASTEC V2.1 major version. *Annals of Nuclear Energy*. Volume 93. pp. 83-93.
- Chatelard, P. & Reinke, N. 2015. Overview of the integral code ASTEC V2.1.0. PSN-RES/SAG/2015-00027. 25 p.
- Chevalier-Jabet, K., Cousin, F., Cantrel, L & Séropian C. 2014. Source term assessment with ASTEC and associated uncertainty analysis using SUNSET tool. *Nuclear Engineering and Design*. Volume 272. pp. 207-218.
- Clément, B. & Zeyen, R. 2013. The Objectives of the Phébus FP Experimental Programme and Main Findings, *Annals of Nuclear Energy*, vol. 61, pp. 4–10.
- Clément, B., Cantrel, L., Ducors, G., Funke, F., Herranz., L, Rydl, A., Weber, G. & Wren C. 2007. State of the Art Report on Iodine Chemistry. Nuclear Energy Agency, Committee on the Safety of Nuclear Installation. NEA/CSNI/R(2007)1. 60 p.
- Clever, H.L. (Ed.). 1979. IUPAC Solubility Data Series, Vol. 2, Krypton, Xenon and Radon. Pergamon Press. Oxford, England.
- Colombani, J., Pascal, C., Martinet, L., Gomez, C. & Bosland, L. 2011. Experimental study of organic iodide formation from painted surfaces in the containment atmosphere during a severe accident. Proceedings of ICAPP2011. Nice, France. May 2-5, 2011.
- Cousin, F. & Jacq, F. 2015. ASTEC V2 ISODOP module. Theoretical manual. PSN-RES/SAG/2014-XX. 26 p.
- Eckerman, K. F. & Ryman, J. C. 1993. External exposure to radionuclides in air, water and soil. Federal Guidance Report No. 12. EPA-402-R-93-081. Oak Ridge National Laboratory.

- Funke, F., Langrock, G., Kanzleiter, T., Poss, G., Fischer, K., Kühnel, A., Weber, G. and Alleleic, H.-J. 2012. Iodine oxides in large-scale THAI tests. Nuclear Engineering and Design. Volume 245. pp. 206-222.
- Gauld, I. C. et al. 2011. ORIGEN-ARP: Automatic Rapid Processing for Spent Fuel Depletion, Decay and Source Term Analysis. Oak Ridge National Laboratories. ORNL/TM-2005/39, version 6.1.
- Girault, N. & Payot, F. 2013. Insights into iodine behaviour and speciation in the Phébus primary circuit. Annals of Nuclear Energy. Volume 61. pp. 143-156.
- Glowa, G. & Moore, C. 2011. Behaviour of Iodine Project, Final Summary Report. NEA/CSNI/R(2011)11.
- Herranz, L. & Clément, B. 2010. In-containment source term: key insights gained from a comparison between the PHEBUS-FP programme and the US-NRC NUREG-1465 revised source term, *Progress in Nuclear Energy*, vol. 52, pp. 481–486.
- Lundgren, K. 2008. Olkiluoto 1 and 2 Periodic Safety Review 2008 - Core Inventories of Fission Products and Actinides, Westinghouse Electric Sweden AB, Report SES 07-096, rev 0.
- Murphy K.G. & Campe, K.M. 1974. "Nuclear Power Plant Control Room Ventilation System Design for Meeting General Design Criterion 19," in Proceedings of the 13th AEC Air Cleaning Conference, CONF-740807, U.S. Atomic Energy Commission, Washington, DC.
- Nieminen A. 2016. Defining dose rates in Nordic BWR containment with ASTEC. Research Report VTT-R-00673-16. 25 p.
- NRC. 1972. U. S. Nuclear Regulatory Commission, Regulatory Guide 1.25, Assumptions used for evaluating the potential radiological consequences of a fuel handling accident in the fuel handling and storage facility for boiling and pressurized water reactors.
- Penttilä, K., Könönen, N. & Rossi J. 2014. The formation of nitric acid inside a BWR containment after severe accident Ver. 2. Research Report VTT-R-01071-14.
- Simondi-Teisseire, B., Girault, N., Payot, F. and Clément, B. 2013. Iodine behaviour in the containment in Phébus FP tests. Annals of Nuclear Energy. Volume 61, November 2013. pp. 157-169.
- Soffer, L., Burson, S.B., Ferrell, C.M., Lee, R.Y. & Ridgely, J.N. 1995. Accident Source Terms for Light-Water Nuclear Power Plants. Final Report NUREG-1465. U.S. Nuclear Regulatory Commission, Office of Nuclear Regulatory Research.
- U.S. Nuclear Regulatory Commission. 2013. Findings and Use of Results from Phébus-FP Tests to Validate the NRC's MELCOR Severe Accident Code and Revised Accident Source Term (NUREG-1465). Research Information Letter (RIL) 1301.
- Viitanen, P. & Palomäki, M. 2011. FSAR / 6 – Radioactive Matter. Revision 3. Teollisuuden Voima Oyj. Tunnus: 129487.
- Weber C.F. 1991. Calculation of Absorbed Doses to Water Pools in Severe Accident Sequences. NUREG/CR-5808. Oak Ridge National Laboratory.

Appendix A.

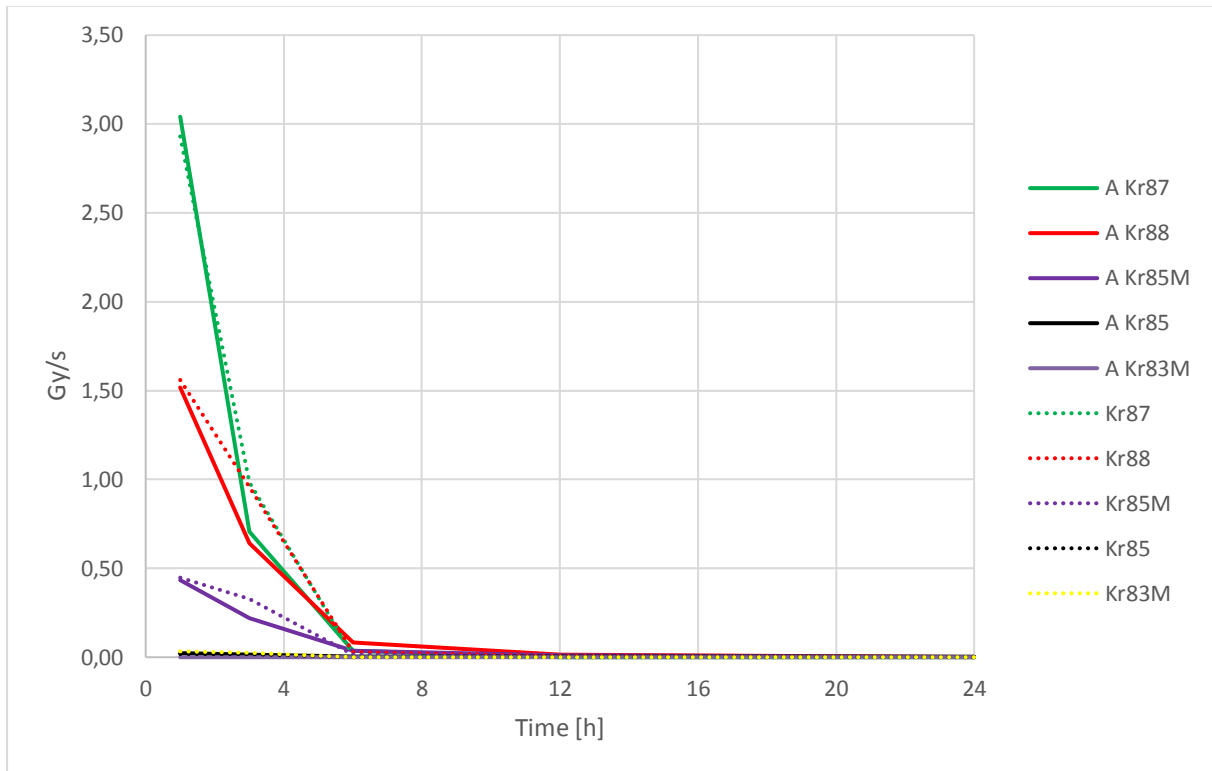


Figure A1. Beta radiation produced by Kr isotopes in the drywell. Solid lines are for ASTEC results and dotted lines for NRC method. To simplify the comparison, only the corresponding time points of ASTEC results with NRC method are depicted.

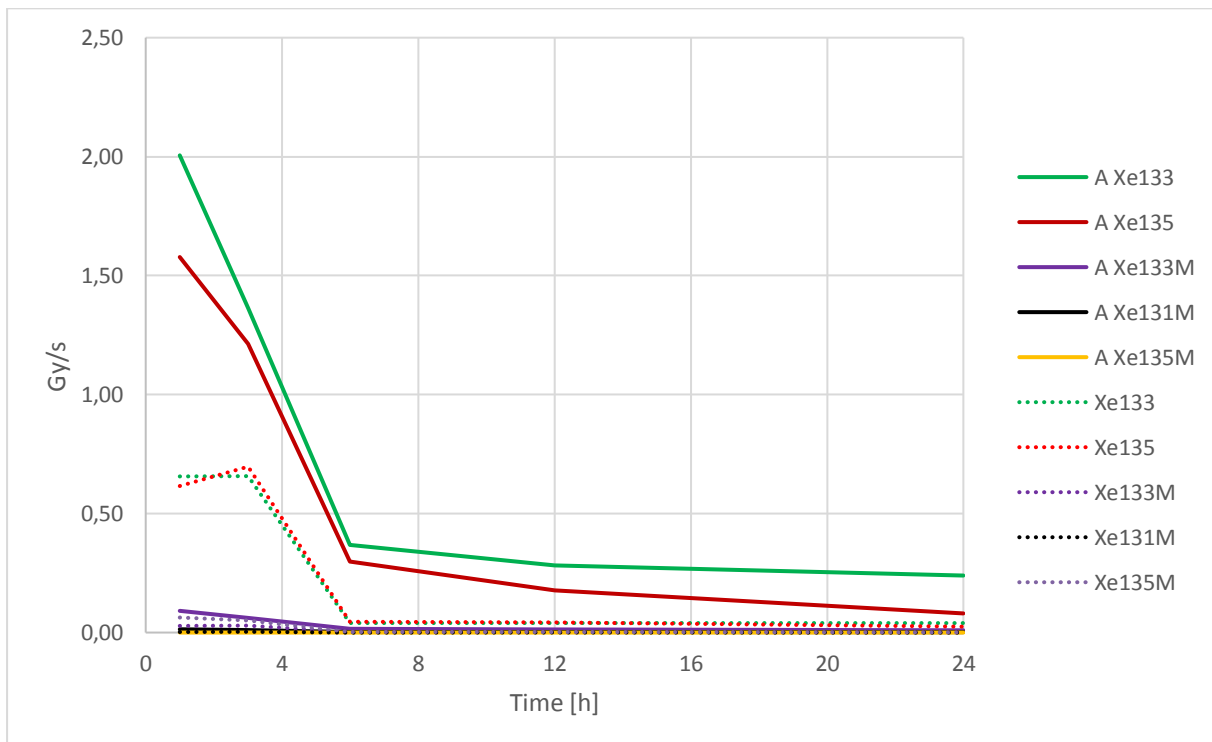


Figure A2. Beta radiation produced by Xe isotopes in the drywell. Solid lines are for ASTEC results and dotted lines for NRC method. To simplify the comparison, only the corresponding time points of ASTEC results with NRC method are depicted.

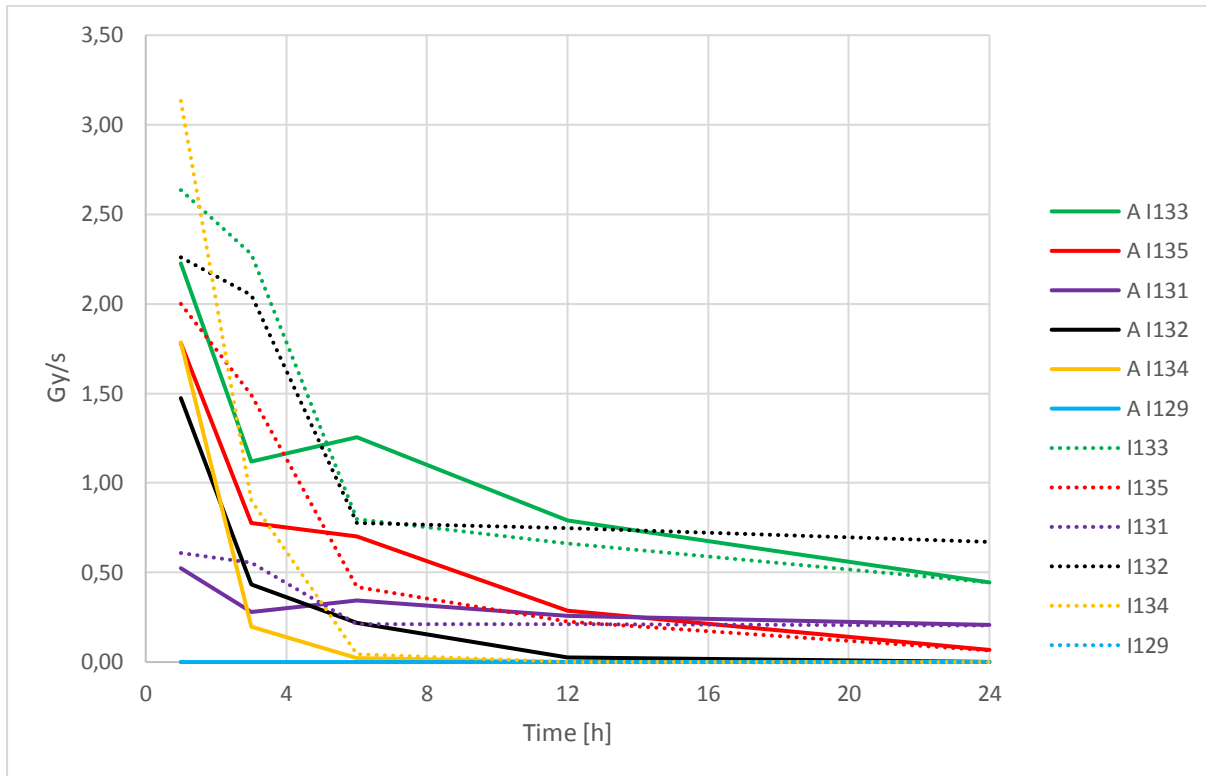


Figure A3. Beta radiation produced by I isotopes in the drywell. Solid lines are for ASTEC results and dotted lines for NRC method. To simplify the comparison, only the corresponding time points of ASTEC results with NRC method are depicted.

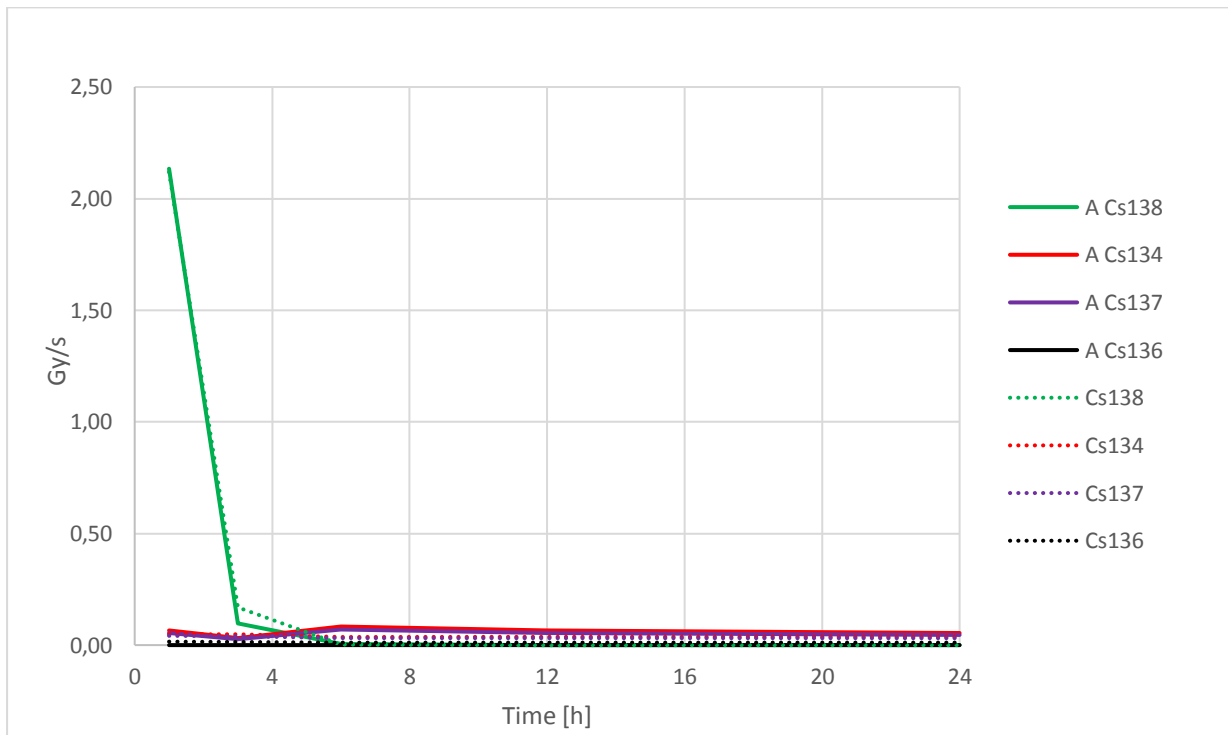


Figure A4. Beta radiation produced by Cs isotopes in the drywell. Solid lines are for ASTEC results and dotted lines for NRC method. To simplify the comparison, only the corresponding time points of ASTEC results with NRC method are depicted.

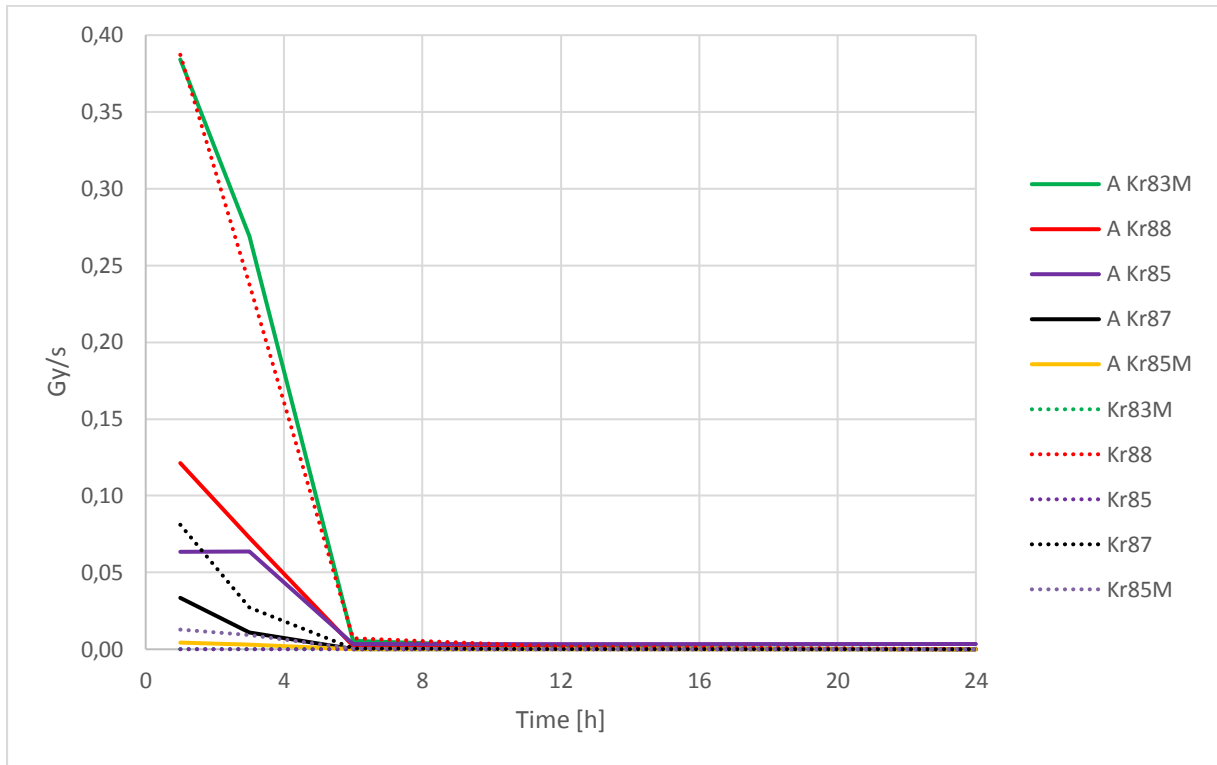


Figure A5. Gamma radiation produced by Kr isotopes in the drywell. Solid lines are for ASTEC results and dotted lines for NRC method. To simplify the comparison, only the corresponding time points of ASTEC results with NRC method are depicted.

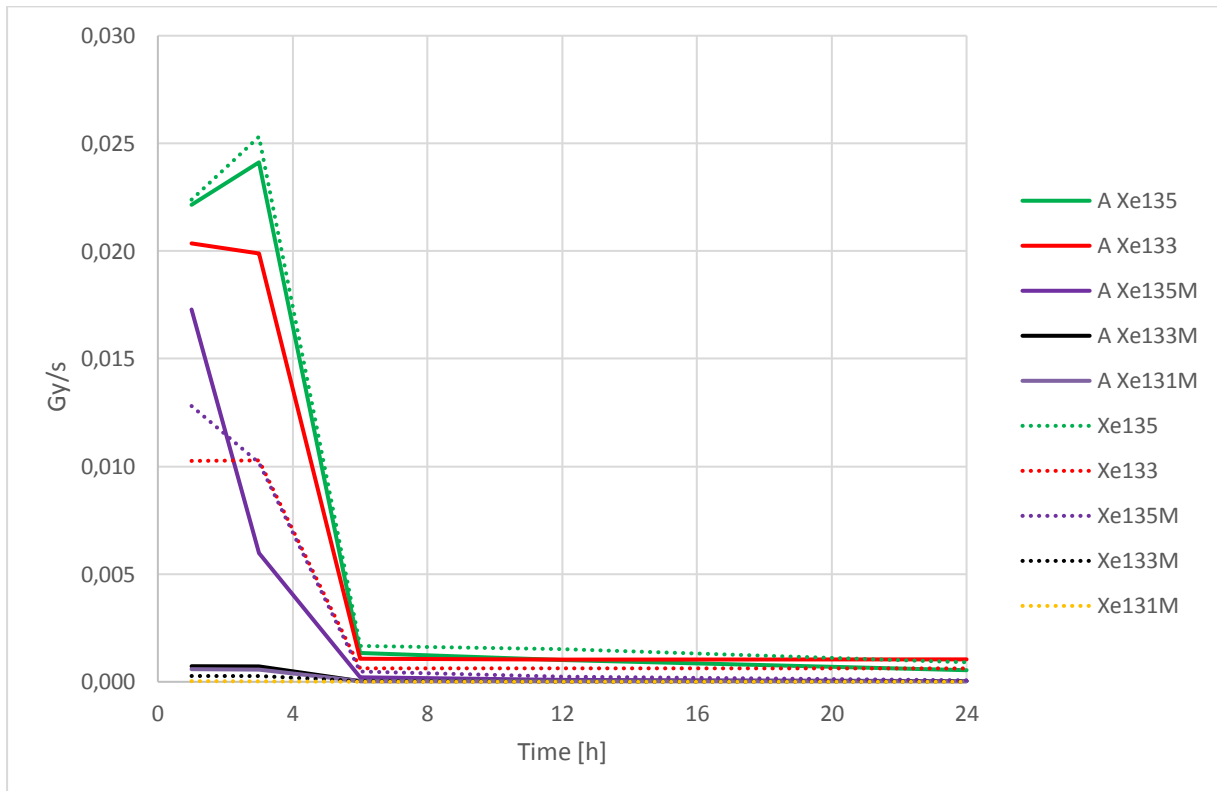


Figure A6. Gamma radiation produced by Xe isotopes in the drywell. Solid lines are for ASTEC results and dotted lines for NRC method. To simplify the comparison, only the corresponding time points of ASTEC results with NRC method are depicted.

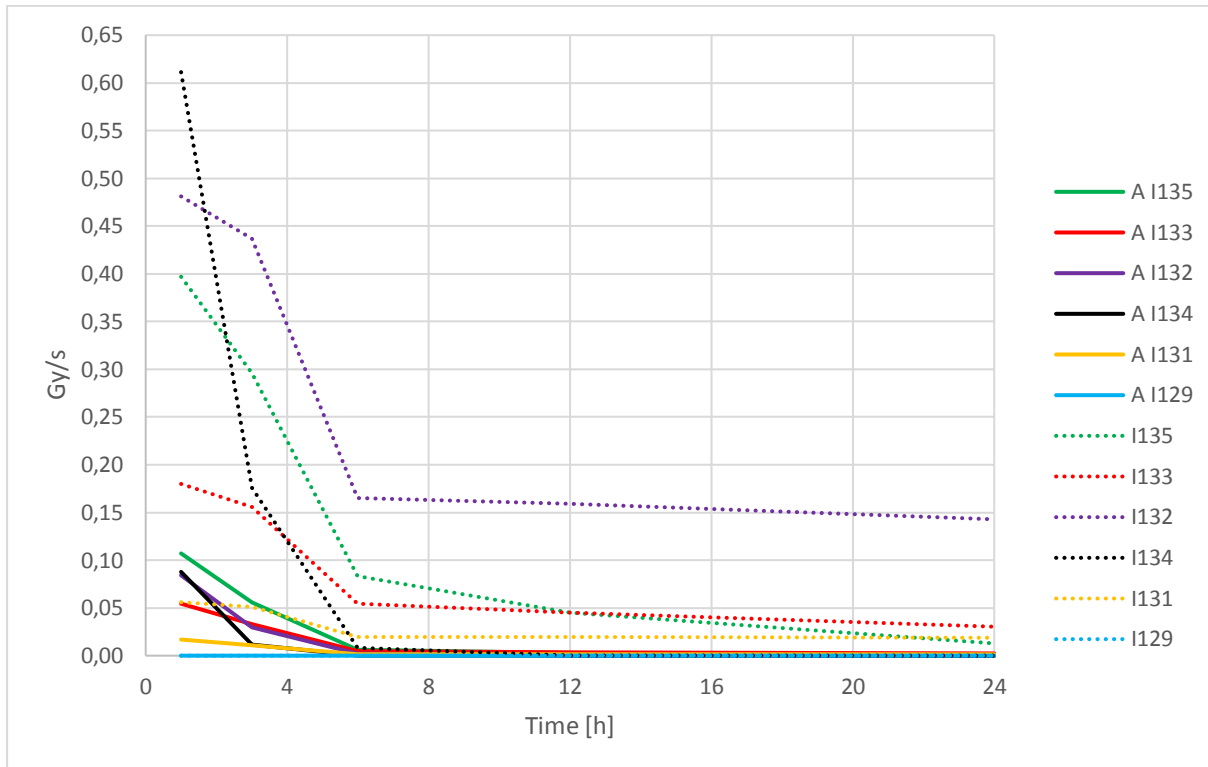


Figure A7. Gamma radiation produced by I isotopes in the drywell. Solid lines are for ASTEC results and dotted lines for NRC method. To simplify the comparison, only the corresponding time points of ASTEC results with NRC method are depicted.

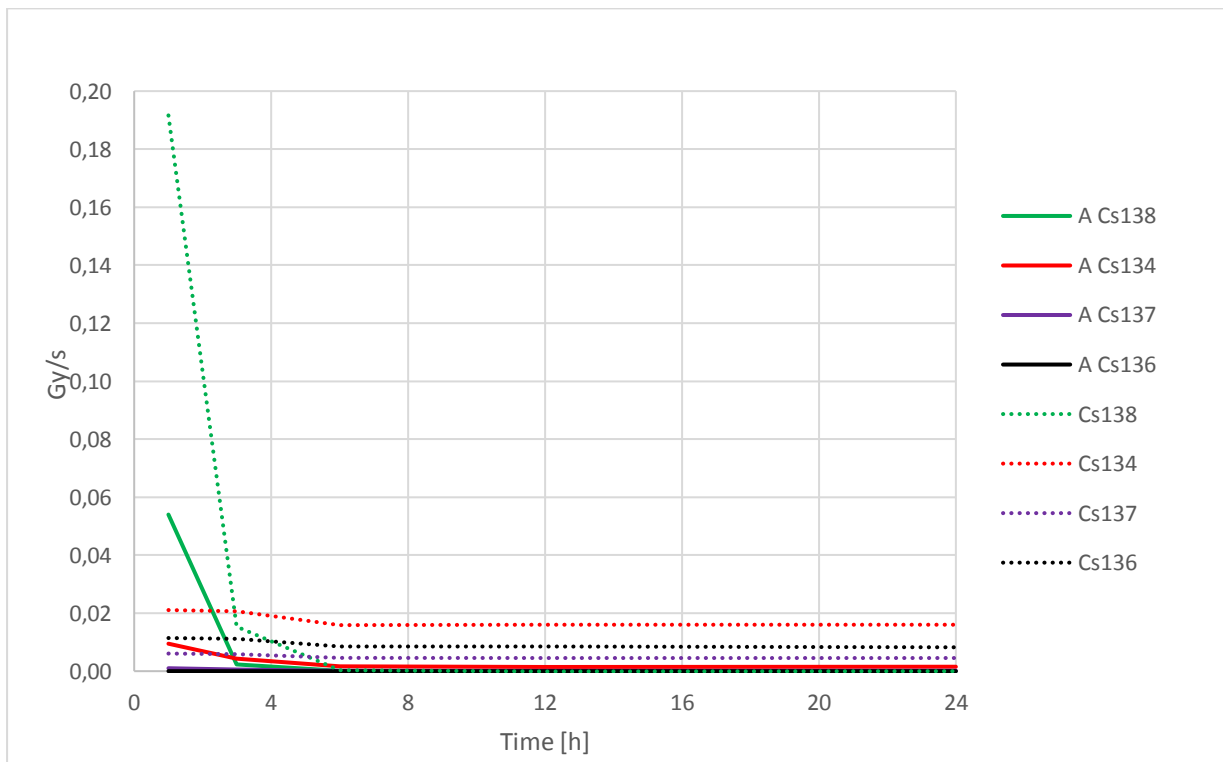


Figure A8. Gamma radiation produced by Cs isotopes in the drywell. Solid lines are for ASTEC results and dotted lines for NRC method. To simplify the comparison, only the corresponding time points of ASTEC results with NRC method are depicted.

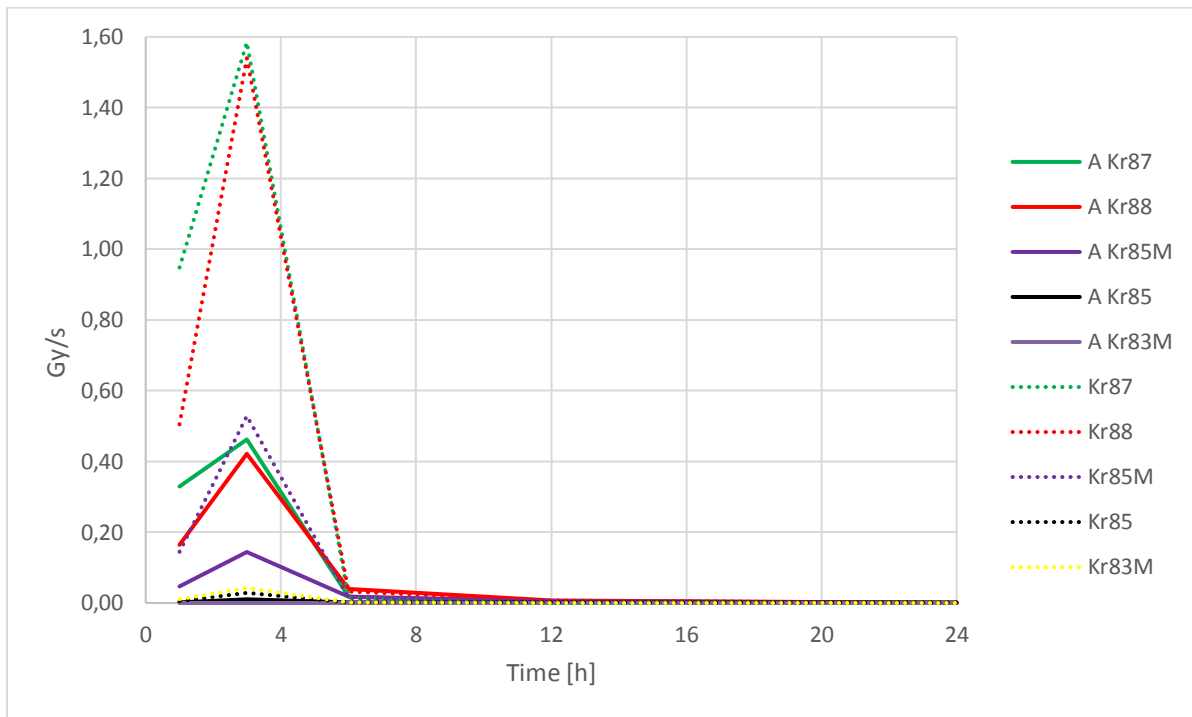


Figure A9. Beta radiation produced by Kr isotopes in the cavity. Solid lines are for ASTEC results and dotted lines for NRC method. To simplify the comparison, only the corresponding time points of ASTEC results with NRC method are depicted.

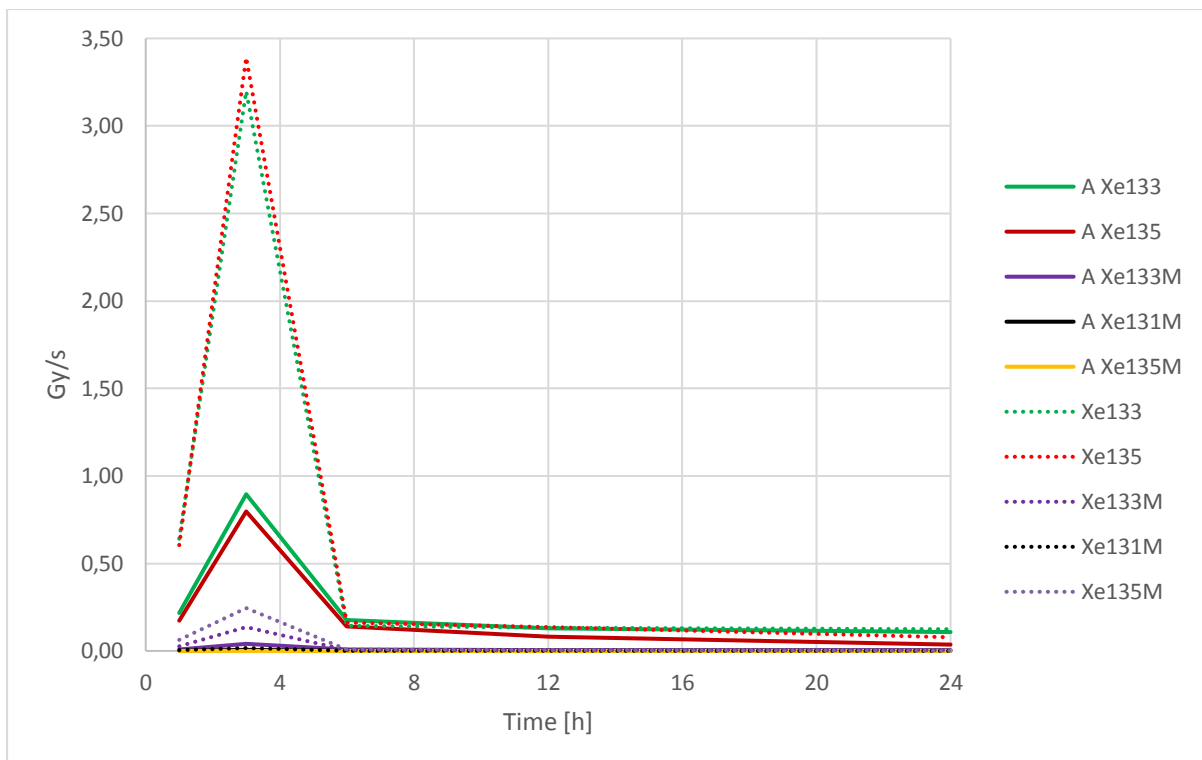


Figure A10. Beta radiation produced by Xe isotopes in the cavity. Solid lines are for ASTEC results and dotted lines for NRC method. To simplify the comparison, only the corresponding time points of ASTEC results with NRC method are depicted.

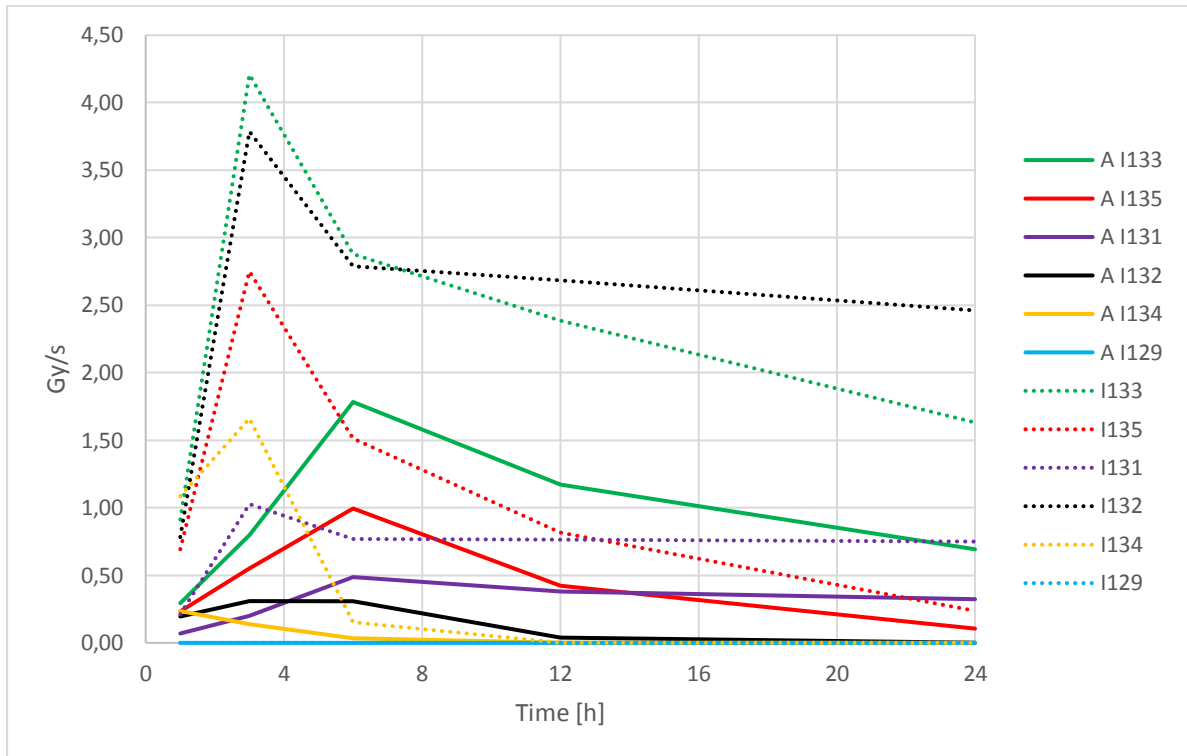


Figure A11. Beta radiation produced by I isotopes in the cavity. Solid lines are for ASTEC results and dotted lines for NRC method. To simplify the comparison, only the corresponding time points of ASTEC results with NRC method are depicted.

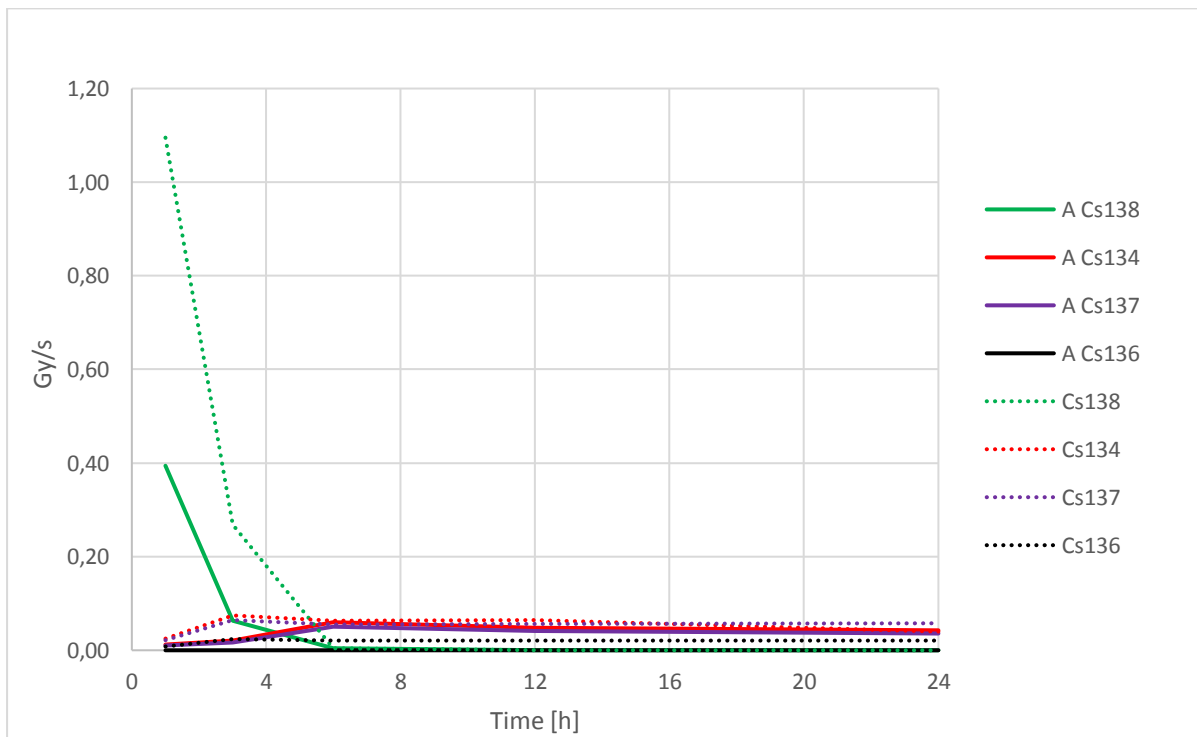


Figure A12. Beta radiation produced by Cs isotopes in the cavity. Solid lines are for ASTEC results and dotted lines for NRC method. To simplify the comparison, only the corresponding time points of ASTEC results with NRC method are depicted.

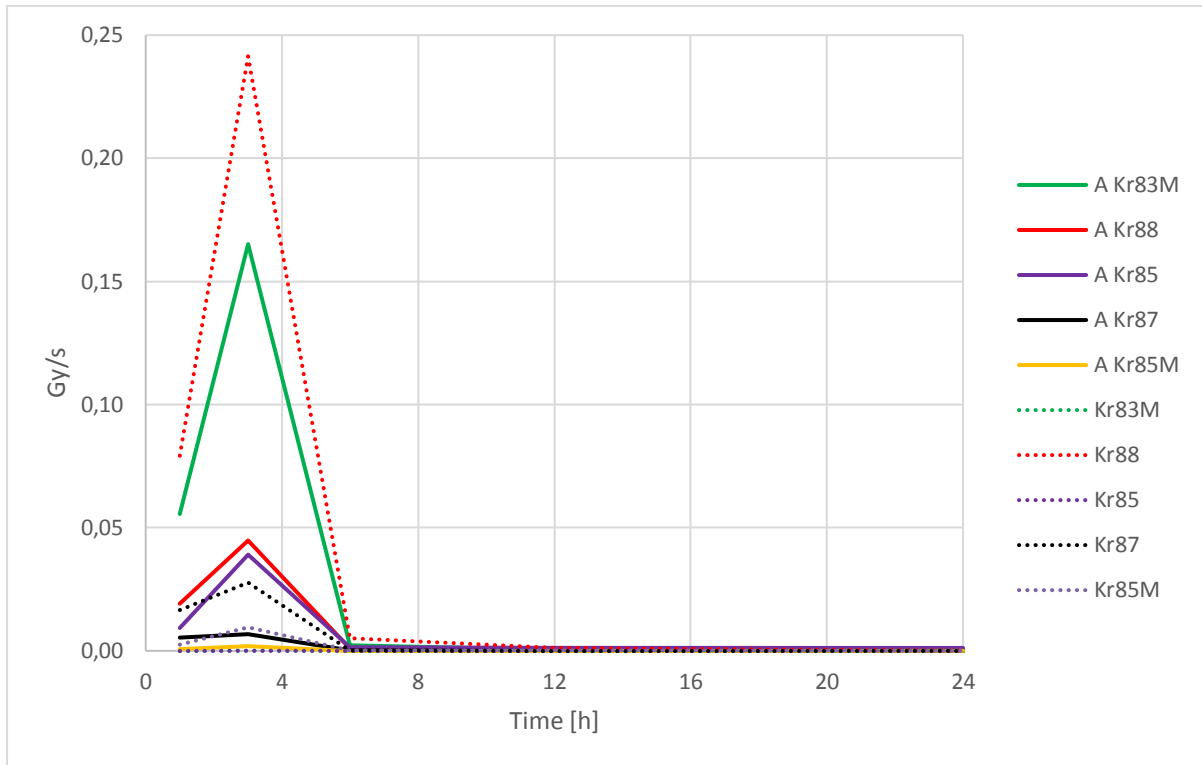


Figure A13. Gamma radiation produced by Kr isotopes in the cavity. Solid lines are for ASTEC results and dotted lines for NRC method. To simplify the comparison, only the corresponding time points of ASTEC results with NRC method are depicted.

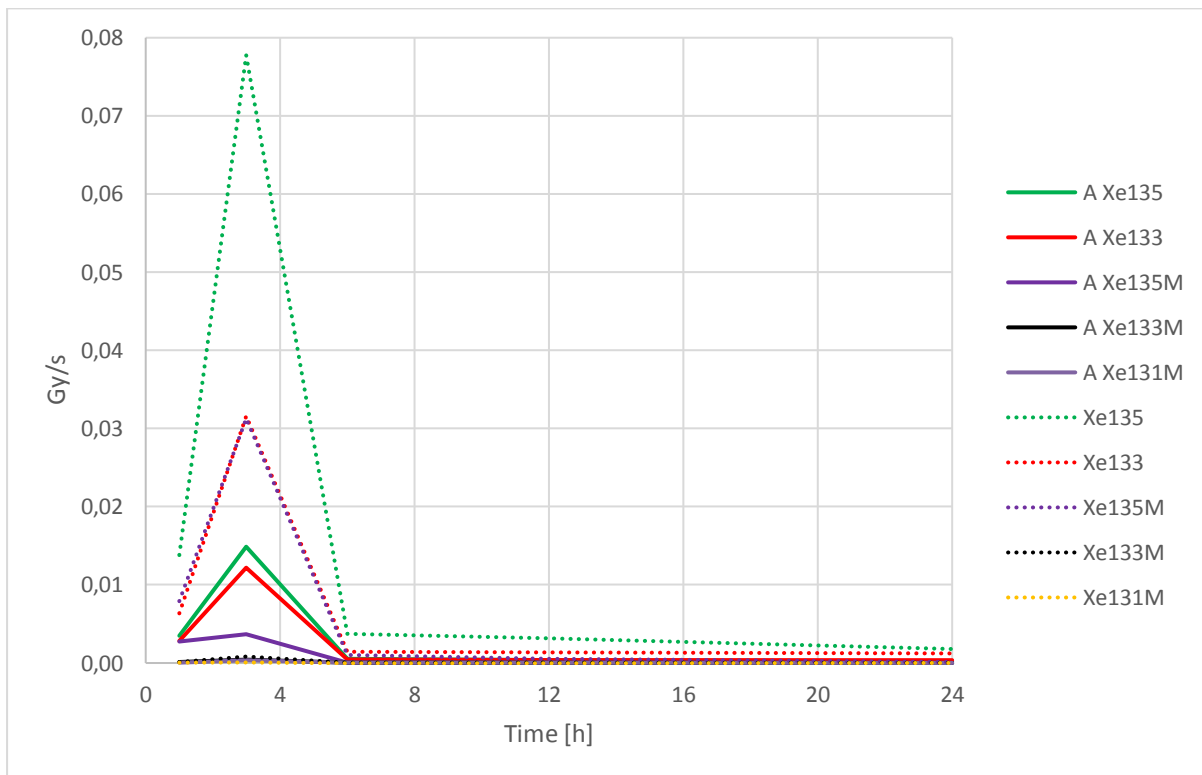


Figure A14. Gamma radiation produced by Xe isotopes in the cavity. Solid lines are for ASTEC results and dotted lines for NRC method. To simplify the comparison, only the corresponding time points of ASTEC results with NRC method are depicted.

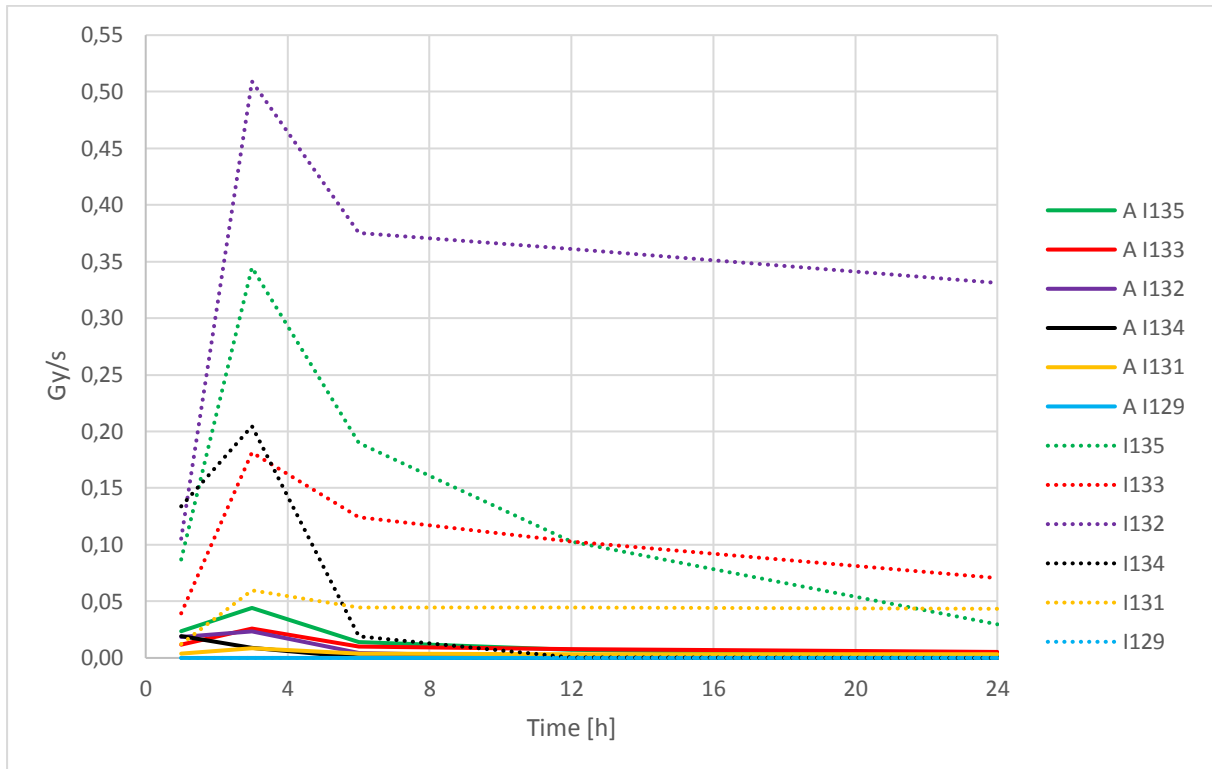


Figure A15. Gamma radiation produced by I isotopes in the cavity. Solid lines are for ASTEC results and dotted lines for NRC method. To simplify the comparison, only the corresponding time points of ASTEC results with NRC method are depicted.

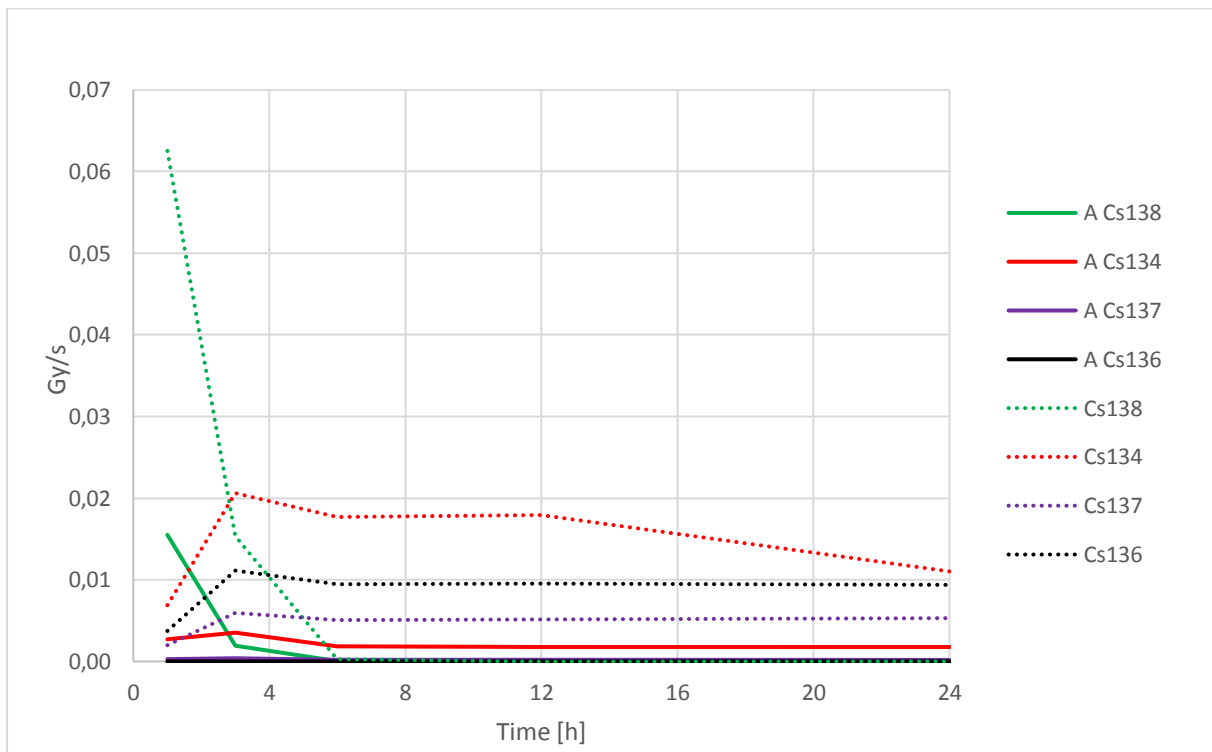


Figure A16. Gamma radiation produced by Cs isotopes in the cavity. Solid lines are for ASTEC results and dotted lines for NRC method. To simplify the comparison, only the corresponding time points of ASTEC results with NRC method are depicted.